Study of Narrow Mesons near Their Thresholds

D. M. Binnie, L. Camilleri,* N. C. Debenham, A. Duane, D. A. Garbutt,
J. R. Holmes, W. G. Jones, J. Keyne, M. Lewis, I. Siotis, and P. N. Upadhyay†
Imperial College, London, England

I. F. Burton and J. G. McEwen
University of Southampton, Southampton, England
(Received 5 April 1973)

A novel form of mass spectrometer has been used to measure the masses, widths, and cross sections of the η, ω, X^0(958), and ϕ mesons near their respective thresholds in the reaction $\pi^- + p \rightarrow$ missing mass $+ n$. The incident momentum is varied in small steps through the threshold while neutrons of a given momentum are detected near zero degrees. The lower limit of the c.m. momentum P^* at which measurements have been made ranges from about 50 MeV/c at the ϕ to about 30 MeV/c at the η. A somewhat low value for the ω mass, 782.3 ± 0.6 MeV, is found. The width of the X^0 is < 1.9 MeV (95% confidence level). All four mesons show evidence of S-wave production, with values of σ/P^* of 21.2 ± 1.8, 0.35 ± 0.03, and 0.29 ± 0.06 μb/(MeV/c) for the η, X^0, and ϕ, respectively. A rapid rise in the ω cross section appears to be modified by a final-state interaction. The effect of this rise can probably be seen in some S_{11} pion-nucleon phase-shift solutions. Evidence is also presented of a sudden drop in the $\pi^+\pi^-$ mass spectrum just above the threshold for the production of a K^+K^- pair. The paper includes a comprehensive discussion of the method and of the details of the spectrometer.

I. INTRODUCTION

The mass spectrum of the nonstrange mesons has been the subject of intensive study. It has been found that several of these mesons are narrow, that is, have widths comparable to or less than typical experimental resolutions. This applies not only to such well-established ones as η and ω, but also to others, in particular a group near 1 GeV, which as yet lack detailed confirmation. We have used a novel form of the missing-mass technique to investigate narrow mesons, in which we exploit the high mass resolution available near the reaction threshold. In this paper we describe the technique and report on the results obtained for the isotopic-spin-zero mesons η, X^0, ω, and ϕ. Some of the results on the X^0 have already been published.[1] The experiment was carried out at the proton synchrotron Nimrod of the Rutherford Laboratory.

The missing-mass technique relies on energy and momentum conservation to determine the invariant mass of a number of kinematically undefined particles. Usually, the mass spectrum is obtained by scanning in one or more of the measured kinematical variables in the final state at a fixed incident momentum. In this experiment the method is reversed; the spectrum is achieved by scanning in the incident momentum, holding constant, within a small range, the measured final-state variables. A particular case of this is the "threshold-crossing" method in which each value of the missing mass is examined by varying the incident momentum across the threshold for its production. In addition to a high-resolution measurement of the masses and widths of the resonances, we have therefore determined the production cross sections very close to threshold. The magnitudes of these vary greatly; the forms of variation also present some interesting comparisons.

In Part II we discuss general aspects of the technique we have used and its relationship to other missing-mass techniques. The experimental implementation of a variable-incident-momentum technique presents certain problems whose solution we believe to be of general interest. These problems are discussed in Part III of this paper, where we also describe the experimental setup and discuss its operation. The method of analysis leading to the determination of masses, widths, and cross sections near threshold are described in Part IV. Finally in Part V we present and discuss our results on the $I = 0$ pseudoscalar and vector mesons.

II. GENERAL CONSIDERATIONS

Consider the reaction $1 + 2 \rightarrow 3 + 4$, where 1, 2, and 4 are relatively stable particles and 3 represents a group of kinematically undefined particles. Let the symbols M, E, P, T, and β, with an ap-

propriate subscript, denote the mass, total energy, momentum, kinetic energy, and velocity of a particle or particle group. Unless specified otherwise, all variables are taken in the laboratory system. Energy and momentum conservation allow the calculation of the invariant mass

$$M_3^2 = M_1^2 + M_2^2 + M_4^2$$
$$+ 2(E_1 M_2 - E_1 E_4 - M_2 E_4 + P_1 P_4 \cos\theta_4). \quad (1)$$

Particle 1 is the beam particle, particle 2 is assumed initially at rest. θ_4 is the polar angle of particle 4 to the beam. The uncertainty in the determination of M_3 can be considered in terms of the three differential coefficients

$$M_3 \frac{\partial M_3}{\partial P_1} = P_4 \cos\theta_4 - \beta_1(E_4 - M_2),$$

$$M_3 \frac{\partial M_3}{\partial P_4} = (E_1 + M_2)(\beta_c \cos\theta_4 - \beta_4), \quad (2)$$

$$M_3 \frac{\partial M_3}{\partial \theta_4} = - P_1 P_4 \sin\theta_4.$$

β_c is the velocity of the center of mass of 1 and 2 in the laboratory. We shall also use in what follows the four-momentum transfer squared, which can be written

$$t = (p_2 - p_4)^2 = (M_4 - M_2)^2 - 2 T_4 M_2,$$

where p_2 and p_4 are the four-momenta of particles 2 and 4.

For a fixed incident momentum the number of events/incident beam particle into a solid angle $\Delta\Omega$ and momentum interval ΔP_4 will be given by

$$R = N_H \int_{\Delta\Omega} \int_{\Delta P_4} \frac{d^2\sigma}{d\Omega d P_4} d\Omega dP_4$$

$$= \frac{N_H}{2\pi} \int \int \frac{d^2\sigma}{dt dM_3} J_P d\Omega dP_4. \quad (3)$$

N_H is the number of target particles/unit area and J_P is the Jacobian for the transformation from $(\cos\theta_4, P_4)$ to the Lorentz-invariant variables (t, M_3):

$$J_P = 2 P_1 M_2 P_4^2 / (M_3 E_4). \quad (4)$$

In general a high-resolution measurement of M_3 requires accurate knowledge of P_1, P_4, and θ_4, however certain kinematic regions can be chosen in which one or more of the differential coefficients in (2) are close to zero, thus reducing the required precision of the relevant variables. This can be exploited either to simplify the experimental design or to improve the mass resolution or both. We first review briefly the various regions under the assumption that P_1 is kept fixed, and then discuss the consequences of allowing it to

vary. For definiteness we shall refer to the reaction $\pi^- + p \to x^0 + n$.

Fixed Incident Momentum

Figure 1 shows equal M_3 lines on the (P_4, θ_4) plane for $P_1 = 1.55$ GeV/c. The general situation, corresponding to the regions marked (a) in Fig. 1, where none of the differential coefficients are close to zero, is not particularly well suited to counter experiments because of the need to make accurate measurements of P_4 and θ_4.

The region where $\partial M_3/\partial P_4$ is near or equal to zero, corresponding to region (b) of Fig. 1, is the so-called Jacobian peak region.[2] It derives its name from the fact that for P_1 and M_3 fixed and $\theta_4 = \theta_{max}$, a small laboratory solid angle corresponds to a large solid angle in the c.m. system. The condition also corresponds to the vanishing of $\partial M_3/\partial P_4$; the events are spread over a wide range of momenta and the Jacobian J_P of Eq. (4) remains finite. For a restricted range of M_3 the property allows a reduction in the size of the detectors while maintaining a good acceptance. For a wider range the main advantage lies in the improved resolution and experimental simplifications arising from the insensitivity to P_4. A further advantage is that by choosing the recoil angle appropriately, it is possible to detect a resonance in missing mass at incident momenta near the peak of the production cross section. Several experiments have used this technique to study the meson spectrum.[3] Typical values of the resolution have a full width at half maximum (f.w.h.m.),
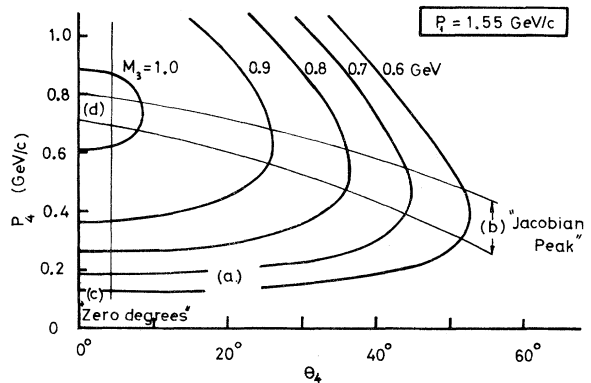

FIG. 1. The relationship between momentum and angle in the laboratory frame at a fixed incident momentum and given values of M_3 in the reaction $1 + 2 \to 3 + 4$. The mass of 3 is to be determined from measurements of 1 and 4. In region (a) both θ_4 and P_4 must be accurately measured whereas in (b) only θ_4 (Jacobian peak) and in (c) only P_4 (zero-degree method). Region (d) is common to both (b) and (c). The curves are drawn for the reaction $\pi^- + p \to x^0 + n$.

ranging from 15 to 25 MeV, for M_3 in the range $700 < M_3 < 1300$ MeV.

The region where $\partial M_3 / \partial \theta_4$ is near or equal to zero, corresponding to region (c) of Fig. 1, is known as the "zero-degree" region since $\partial M_3 / \partial \theta_4 \to 0$ as $\theta_4 \to 0$. The main advantage of exploiting this region is that accurate measurements of θ_4 are not required. This is particularly helpful for neutrons. Assuming that P_4 is to be measured by timing the neutron over a fixed distance d then the mass spectrum will be derived from the neutron time-of-flight spectrum $N(\tau)$. This is related to $d^2\sigma/dt dM_3$ by the expression

$$N(\tau) = \frac{dR}{d\tau}$$

$$= \frac{N_H}{2\pi} \int_{\Delta\Omega} \frac{d^2\sigma}{dt dM_3} J_\tau d\Omega \qquad (5)$$

(events/nsec)/incident pion,

where

$$J_\tau = 2P_1 M_2 P_4^4 c/(M_3 M_4^2 d)$$

and   (6)

$$\tau = \tau_4 - \tau_0 = (1/\beta_4 - 1)d/c,$$

J_τ being the transformation Jacobian between (M_3, t) and $(\cos\theta_4, \tau)$ and τ the time of flight in nsec relative to a reference time τ_0 corresponding to the arrival of particles with $\beta_4 = 1$.

Figure 1 shows that at zero degrees each missing-mass value is collected at two points corresponding to the recoil nucleon going forward and backward in the c.m. system and therefore having maximum and minimum values respectively of t. The requirement of high resolution implies working with backward going nucleons and this is where the method has usually been applied. Unlike protons, neutrons suffer no energy loss in the target so that P_4 is given directly in terms of τ. Note that if t channel exchange is important, then depending on the reaction, $d\sigma/dt$ may be abnormally high or low in this region.

A general disadvantage of the method is that the time-of-flight spectrum given by (5), which is almost linearly related to the mass spectrum, falls rapidly with increasing time-of-flight. The decrease is dominated by the Jacobian factor which from (6) is seen to fall like P_4^4. This rapid variation in the nonresonant background makes the unambiguous recognition of a small resonance effect very difficult. Although in principle the factor can be removed during analysis, in practice difficulties arise. The main problem is that there may be other contributions to the counting rate. Thus a relatively flat background which could be

produced by accidental coincidences, would be transformed into a rapidly rising spectrum of uncertain shape. Note however that much information can be gained if the run is split into two or more parts, at slightly different incident momenta, so that the mass scale is displaced but the general background shape essentially unaltered. The systematic application of this idea is one of the features of the present experiment.

The zero-degrees method has been used for the study of both charged and neutral missing-mass systems.[4] For $900 < M_3 < 1300$ MeV, typical values of the resolution have a f.w.h.m. in the range from 10 to 15 MeV.

Variable Incident Momentum

As can be seen from Fig. 1 the Jacobian peak region (b) and the zero-degree region (c) coincide in the threshold region (d). Here the conditions $\partial M_3 / \partial \theta_4 \to 0$ and $\partial M_3 / \partial P_4 \to 0$ are simultaneously satisfied. For these coefficients to vanish we require $\theta_4 = 0$ and $\beta_4 \sec\theta_4 = \beta_c$. Thus in the limit, particle 4 is at rest in the c.m. system and for a given P_1, M_3 has its maximum possible value.

There are several difficulties in trying to exploit this region at a fixed beam momentum. The vanishing of $dM_3/d\tau$ implies a high degree of nonlinearity of the mass scale and of the acceptance as a function of missing mass. Also the P_4^4 factor in the Jacobian referred to above leads to an extremely rapid variation in the nonresonant background spectrum. However all these can be avoided and the high-resolution property of the threshold region maintained, if M_3 is varied by varying P_1 in very small steps. For each value of missing mass, the corresponding recoil nucleon will then be detected as P_1 crosses a momentum just above the threshold for its production. We refer to this as the "threshold-crossing" technique.

The kinematics of the threshold-crossing region are shown in Fig. 2 which shows M_3 contours on the $P_1 P_4$ plane for $\theta_4 = 0$. The main characteristics of this region are discussed below.

Experimental Aspects

The incident momentum, which defines the missing mass, can be chosen so as to concentrate the data in a narrow mass region of particular interest. It can be measured with high accuracy by a momentum spectrometer and hodoscopes and is easily computed using hardware logic. In the present experiment the momentum step was chosen to be 0.5% of P_1. This defined a momentum scale of the form $P_n = P_0 (1.005)^{n-1}$, where P_n is the central momentum of the nth momentum bin. P_0 was taken as 600 MeV/c. The mass spectrum can be
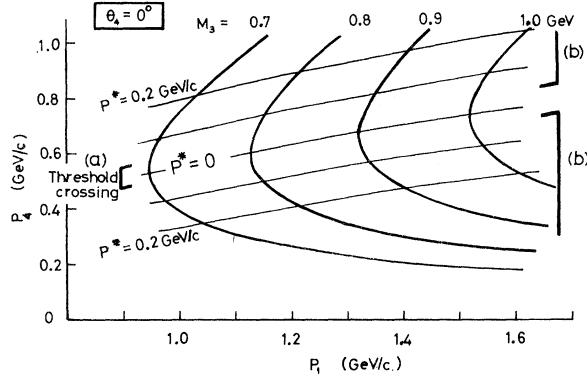
FIG. 2. The systematic variation of P_1. The relationship between P_1 and P_4 at $\theta_4 = 0$ for various values of M_3 and final-state c.m. momentum $P*$ is also shown. Highest resolution is available in region (a), the threshold-crossing region, where in the limit the missing mass depends only on P_1. Region (b) where both P_1 and P_4 must be measured, the hybrid region, is also useful.

obtained by measuring the event rate in a predetermined time-of-flight gate, which may if necessary be varied along with the incident momentum, to cover a wide missing-mass range. Experimentally, the main requirements are clear. Firstly, it must be possible to set the beam rapidly and precisely to any given momentum within the range of interest. Secondly, the apparatus must be stable and the counting rates reproducible, preferably over a period of weeks.

Mass Resolution

Use of data in this kinematical region allows the highest possible resolution in the measurement of M_3. As will be described later we have used a simple incident beam momentum spectrometer to achieve $\Delta P_1 = 0.5\%$ P_1(f.w.h.m.). In the X^0 threshold region near $P_1 = 1.4$ GeV/c this leads to a limiting resolution of $\Delta M_3 \approx 3.5$ MeV (f.w.h.m.). To achieve this figure would imply also a short hydrogen target, small neutron counters and a narrow time-of-flight gate. All these requirements reduce the event rate and in practice all were relaxed to obtain a resultant figure of about 5 MeV at the X^0.

Mass Scale and Counting Rates

At threshold the differential coefficient $\partial M_3 / \partial P_1$ reduces to $\beta_1 M_2 / (M_3 + M_4)$ and is therefore almost constant, typically about 0.5, in the neighborhood of a narrow resonance. Thus there is an almost linear relationship between the momentum scale and the missing-mass scale. The expression for the Jacobian J_τ shows that for given t or P_4 its

variation with P_1 is also slow. Therefore, from (5), the variation with P_1 in the number of events falling within a given interval of P_4 will be dominated by the behavior of the cross section $d^2\sigma / dt dM_3$. If no resonance is present, a smooth, slowly varying rate can be expected. This behavior is in general agreement with observation. Thus we can with this technique study possible resonances, with high mass resolution, in a linear mode and with a nearly constant background.

Description of Resonance Production

As threshold is approached from above, the range of four-momentum transfer kinematically accessible falls, and it is easy to show that $|t|_{\max.} - |t|_{\min} = 4K*P*$, where $K*$ and $P*$ are the initial and final c.m. momenta. $K*$ shows little variation. Thus a constant $d\sigma / dt$ corresponds to an S-wave production cross section, $\sigma = AP*$, where $A = 4K* d\sigma / dt$. So although σ falls, $d\sigma / dt$, which determines the event rate, remains finite. This is the usual assumption made about cross sections near threshold unless some dynamic mechanism which strongly inhibits S-wave production is involved. This possibility is considered in more detail later. It is important that apart from the finite range of the $\pi^- p$ interaction, the initial state places no restriction on the final spin-parity of a meson produced in an S wave.

To describe the resonance we start from the assumption that for a narrow resonance the cross-section behavior with $P*$ and $\theta*$ of each mass interval within the resonance is the same. In terms of t this implies that we can factorize the M_3 and t dependence of the double-differential cross section in (5).

$$\frac{d^2\sigma}{dt dM_3} = \frac{\Gamma/2\pi}{(M_3 - M_0)^2 + (\frac{1}{2}\Gamma)^2} \frac{d\sigma}{dt}, \tag{7}$$

where M_0 and Γ are the central mass and width. As the resonance is assumed narrow we have used the simple Breit-Wigner expression. The implication of the factorization is that if we hold constant the final-state parameters, such as t and θ_4, and scan through M_3 by scanning P_1, we will trace out the form of the resonance independent of any assumptions about cross-section behavior. This is essentially the method we have used to determine the resonance mass and width. Alternatively, by integrating over P_1, and therefore M_3, we can extract the value of $d\sigma / dt$ at various intervals of t. Details of these methods are discussed in Part IV. The possibility of extracting resonance parameters from the threshold region has been discussed by Baz.[5] A variation on the present approach was used by Jones *et al*.[6] to put an upper limit of 0.9 MeV on the η width.

Direct-Channel Effects, Nucleon Isobars

As P_1 is varied, so is the c.m. energy. s-channel resonances could affect the data in various ways. We distinguish two main possibilities. The first is the simple formation of an N^* followed by its ultimate decay, possibly via further N^*'s, into a nucleon and pions. This process leads to a modulation of $d^2\sigma/dtdM_3$, and the event rate, with P_1 and therefore could simulate meson production near threshold. However for narrow resonances the two can be readily distinguished; such an N^* would be characterized by a vertical band on Fig. 2 and the behavior above the assumed threshold would be quite different. The second possibility is that the N^* could be an intermediate state in the formation of the final meson and nucleon. A good example of this is η production via N^* (1535) decay.[7] In addition to the modulation imposed on $d^2\sigma/dtdM_3$, this may lead to constraints on the angular momentum of the final state. In view of the angular momentum barrier effect, such a constraint would have a marked effect on $d\sigma/dt$ near threshold. Thus cross-section measurements near threshold may give useful information on the properties of N^* resonances.

Final-State Interactions

The low value of the c.m. momentum P^* may lead to final-state interactions between the meson resonance or its decay products and the recoil nucleon. If the condition

$$P^*\hbar/M_0\Gamma c^2 < 1 \text{ fermi} \tag{8}$$

is satisfied, the decay will take place within a distance of the order of one fermi from the interaction point. The resonance will never have existed

as a free state outside the field of the nucleon and one might observe forbidden transitions or width changes in analogy with similar effects in optical spectroscopy.[8] In addition the resonance decay products may scatter off the recoil nucleon, leading to further changes in the observed width and the branching ratios into different decay channels.

Of the four resonances investigated the ω is the most suitable for the study of these effects. This is mainly because with a width of about 10 MeV the condition above is satisfied for $P^* \approx 40$ MeV/c, roughly the lower limit of P^* used. In this situation we regard (7) as a parameterization of $d^2\sigma/dtdM_3$, accepting that Γ and possibly M_0 may be functions of P^* or t. Further discussion of these effects is deferred to Sec. V.

Extension into Region Where $\partial M_3/\partial P_4$ Is Not Small

This corresponds to region (b) of Fig. 2. The kinematical properties of this region were discussed in connection with the zero-degree method at fixed P_1. Although it is now possible to produce a mass spectrum with P_1 fixed, the systematic variation of P_1 offers significant advantages which may offset the extra complication involved in the procedure. Figure 3 shows how a mass spectrum is constructed from a series of time-of-flight spectra. The mass intervals have been matched to the momentum intervals and can conveniently be labelled by the momentum bin number closest to threshold. They are then identical to those used in the threshold-crossing technique. Note that each mass bin contains just sufficient contributions for these to be recombined to build up a complete time-of-flight spectrum. Thus the nonresonant background level is almost unaffected.
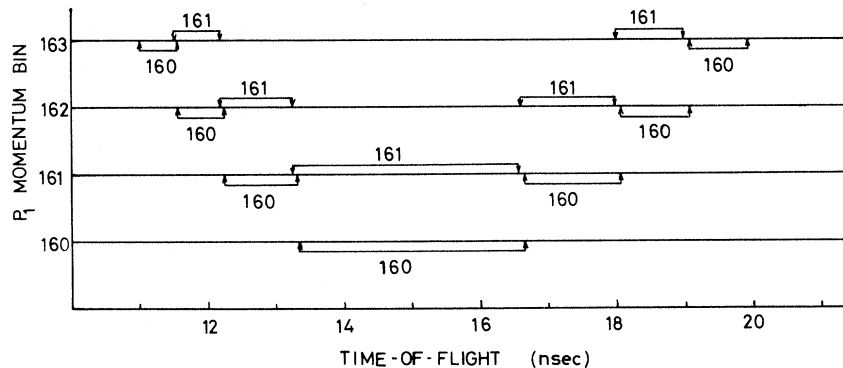

FIG. 3. Data consist of a series of time-of-flight spectra taken at 0.5% intervals of P_1. In the threshold crossing technique the number of neutrons within a narrow time-of-flight gate around the threshold velocity is determined as P_1 is varied. The P_1 scale thus defines an M_3 scale. This is extended into the hybrid region above threshold by adding in the appropriate contributions from the higher momenta. The figure shows the formation of mass bins 160 (900.3 to 903.6 MeV) and 161 from the spectra at momentum bins 160 (1326 MeV/c) to 163 (1346 MeV/c). Note that all times-of-flight contribute to each mass bin and that the background level is therefore unaffected.

As before, all differential coefficients and the Jacobian (6) are only slowly varying functions of P_1, and therefore again any meson resonance should be seen on a relatively flat background. Also as the range of P_4 is constant, so is the detection efficiency for neutrons and the effect of ionization loss in the hydrogen target for protons. For the same reason, any spurious structure always occurring with the same amplitude at a particular time of flight would not appear in the mass spectrum.

In the experiment reported here we have used data in the threshold region for high-resolution width measurements and have followed the resonance into this hybrid region, mainly in order to study the cross-section behavior.

III. EXPERIMENTAL TECHNIQUE

The missing-mass spectrometer was designed to work in the neighborhood of the reaction thresholds

$$\pi^- + p \rightarrow (MM)^- + p, \ (MM)^0 + n$$

for incident momenta between 0.7 and 4.0 GeV/c. Incident pions, of precisely defined momenta, were directed on to a liquid hydrogen target. Secondary nucleons were detected near zero degrees and their momenta determined by a time-of-flight technique. Apart from the lower detection efficiency for neutrons, close to threshold where the laboratory nucleon momentum was high there was little difference in the response to protons and neutrons. Events in the various decay channels could be classified by a system of counters called decay counters which surrounded the hydrogen target. The general layout is shown in Fig. 4.

The beam momentum was defined by a momentum spectrometer included in the beam line and determined with $\Delta P_1/P_1 = 0.5\%$. It was varied in steps of 0.5% and data were accumulated over a wide momentum range. The hydrogen was contained in a melinex flask 29.4-cm long and 6-cm in diameter and the whole encased in a thin walled (mainly 1.5 mm) duralumin cylinder with melinex end windows. The hydrogen was maintained at constant pressure of about 1.07 atmospheres; this determined its density to be 0.070 g/cm^3. The outer cylinder was surrounded by six target counters $T1-6$ made of strips of scintillator 5-cm wide and 3-mm thick wrapped toroidally around the outer cylinder. Their main function was to locate approximately the interaction point inside the target.

Noninteracting beam particles were eliminated from the final trigger by veto counters $V1$ and $V2$, situated at 3 m and 6 m downstream of the hydrogen target. Some problems were experi-
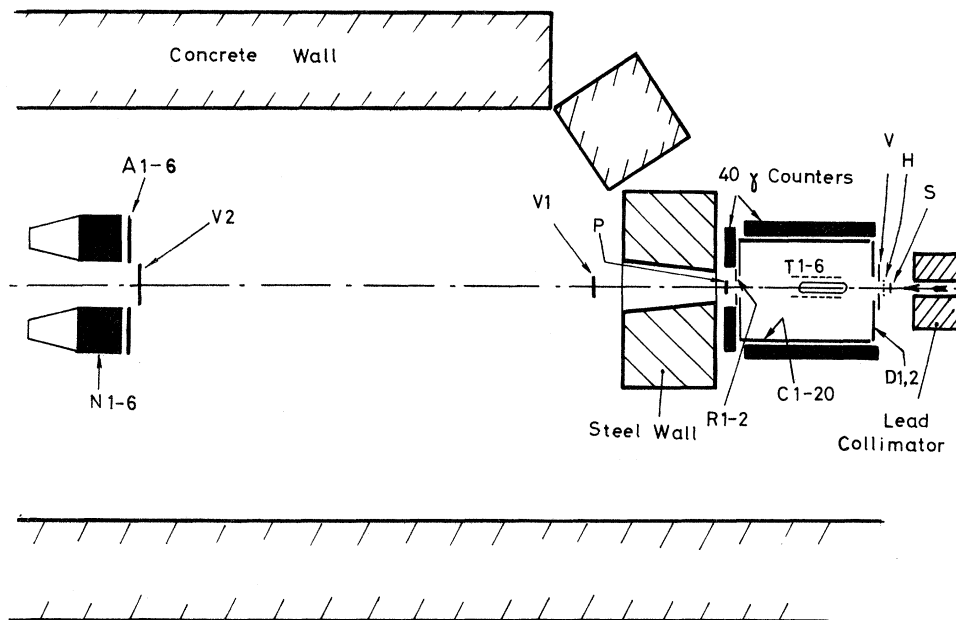

FIG. 4. (Not drawn to scale.) The general layout, excluding the beam. Incident π^- mesons enter from the right and either interact in the hydrogen target or are vetoed by counters $V1$ and $V2$. Neutrons and protons produced at a small angle (1.6–4.4°) may enter one of the six cylindrical neutron counters $N1-6$ and are distinguished by counters $A1-6$ and counter P. Secondary mesons and gamma rays are detected by 66 counters almost surrounding the hydrogen target.

enced with spurious neutron triggers, probably arising from secondary interactions of the original reaction products from the hydrogen in the decay counters, walls etc. These effects were appreciably reduced by a steel wall about 120-cm thick placed as shown in Fig. 4. No analogous problem existed with proton induced triggers. A 2-mm thick scintillation counter P, just downstream of the decay system, the data from which were always recorded, could be set in coincidence (protons) or veto (neutrons) in the analysis.

The slow neutrons and protons were detected by counters $N1-6$ and distinguished by counters $A1-6$. The N counters were cylinders of plastic scintillator arranged symmetrically around the beam axis with their centers at a radius of 32 cm. The upstream face of the counters was positioned 600-cm downstream of the hydrogen target center. The time of flight was determined between a beam counter S and the neutron counters. One of the minor differences between the two nucleons was the effective flight path, about 615 cm on average for neutrons, whereas either 630 or 600 cm for protons depending on the relative velocities of the proton and of scintillation light inside the counter. In general the counters are referred to as neutron counters and will be discussed mainly in this context.

In the remainder of Sec. IV, we discuss in more detail the beam, the neutron counters, the decay system, the electronics, and finally data collection and reduction.

Beam and Momentum Spectrometer

The beam magnets, counters and electronics were designed to produce a measured flux of beam particles having a known, narrow momentum profile. The disposition of the beam elements is shown in Fig. 5. Negative particles from an internal target near the end of a Nimrod octant were transported to an intermediate horizontal and vertical focus near the collimators at G where a rough momentum selection was made. Electrons in the beam were rejected by a threshold gas Čerenkov counter. The second part of the beam also served as a double-focusing momentum spectrometer. Just upstream of the intermediate beam focus was mounted a counter hodoscope, the G hodoscope, consisting of nine fingers each 7.5-mm wide and 5-cm high. After crossing these the pions entered a vacuum pipe, were deflected by the spectrometer dipole $M2$ and focused on to the hydrogen target. A second hodoscope consisting of five fingers each 6.8-mm wide was placed 50-cm upstream of the hydrogen target in such a position that, at the central momentum, the H hodoscope counters and the image of the G hodoscope counters were in coincidence in the horizontal plane, i.e., the hodoscopes were in conjugate planes and the horizontal magnification equalled the ratio of the widths of the counters. The determination of the momentum of a particle was then made directly in terms of its positions in the two hodoscopes and was independent of multiple scattering in the counters. The spectrometer had a dispersion of 0.5% of P_1 per counter width. Five adjacent momentum bins, at 0.5% intervals of P_1, were selected from the beam by conventional fast electronic logic, which formed and ordered coincidences between 25 pairs of counters. A counter S near the hodoscope gave a timing signal and, together with a counter V which surrounded the
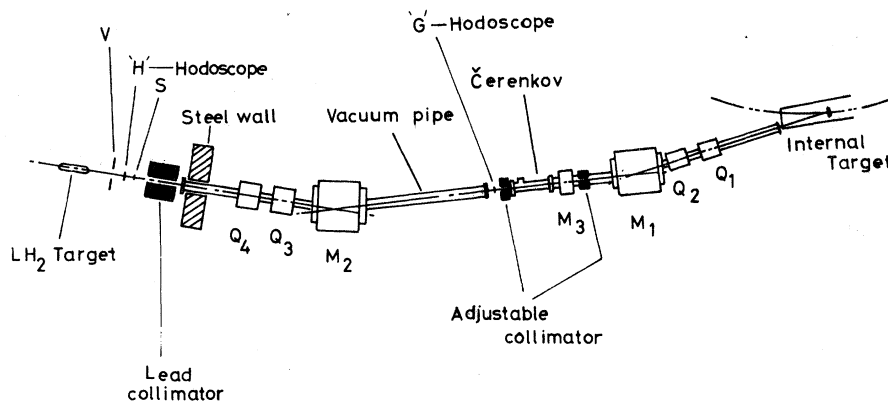

FIG. 5. (Not drawn to scale.) Negative particles from an internal target are deflected and brought to an intermediate focus near the G hodoscope and a final focus at the hydrogen target. Any vertical misalignment could be compensated with the dipole $M3$. Electrons are rejected by a threshold Čerenkov counter. The second half of the beam also acts independently as a precision momentum spectrometer in which the momentum of a particle is determined by its relative positions in counter hodoscopes G and H. Several collimators are used to remove stray beam particles which otherwise could ultimately enter the decay array or the neutron counters. The general shielding of the accelerator is not shown.

beam at S, was also used to reject automatically all particles if two or more were present within any period of about 40 nsec.

The spectrometer magnets were investigated individually using search coils and appropriate shims added. The dipole field was monitored by means of an nuclear magnetic resonance (NMR) probe, and the quadrupole fields by the currents in the windings after cycling to remove hysteresis effects. Magnet supplies were typically stable to better than 1 part in 10^3, and for the spectrometer dipole to 1 part in 10^4. The spectrometer was adjusted and calibrated at a series of momenta from 700 MeV/c to 4 GeV/c using the floating wire technique.[9] An air-bearing pulley removed the usual main source of error in this method. The errors in the absolute current and tension in the wire were estimated to be 1 and 3 parts in 10^4, respectively. Over the range of beam angles of interest, the envelope of the spot size at H from a point source at G was about 1 mm for a wire current corresponding to the central momentum. The calibration was repeated at the end of the experiment and showed a systematic increase of about 0.17% over the original settings. This was mainly attributed to small relative movements of the quadrupoles and hodoscopes. The mean calibration has been used.

If the hodoscope counters were uniformly illuminated, and aberrations neglected, each momentum bin selected by the electronic logic would have a triangular momentum profile with a width of 1% of P_1 across the base. The effect of nonuniform illumination was much reduced as several pairs of counters formed each momentum bin and could be further reduced by collecting data at 0.5% intervals of the central momentum so that each momentum bin had comparable contributions from all five momentum channels. Chromatic aberration in the two outermost momentum channels produced a distribution at the H hodoscope from a point source at G with a standard deviation of about 2 mm. This was the most serious aberration in the spectrometer. Its effect could be reduced by arranging that all five channels contributed to each momentum bin.

The beam was operated typically at an intensity of about $(1.5–2) \times 10^5$ useful pions/pulse with a pulse duration of about 300 msec. At the hydrogen target the f.w.h.m. of the beam was about 3 cm in the horizontal plane and 1 cm in the vertical. Horizontally the beam was almost parallel, vertically the f.w.h.m. of the divergence was about 23 mrad. A correction was made for the small percentage of μ mesons in the beam.

Of the seven magnets, the settings of the three which formed the momentum spectrometer were predetermined from the floating wire measurements. The currents in the two upstream quadrupoles, which controlled the beam shape and angular spread, had been optimized at a series of momenta and were then interpolated. A small vertically deflecting dipole, M_3, was usually unnecessary. This left only one dipole to be optimized at each setting. The beam momentum could be changed in about 15 min. Typically a run lasted about three hours.

Neutron Counters

Each of the six neutron counters consisted of a right cylinder of NE 102A plastic scintillator, of diameter and length 30 cm, viewed from the downstream end through a tapered light guide 30-cm long by a 58AVP photomultiplier. The over-all tube voltage was maintained to within ± 1 volt and the temperature, which also affected the tube gain, to ± 1 °C. For each counter the arrival time of the output pulse was determined by one discriminator and the threshold amplitude defined by a second which had half the sensitivity of the first. Scattered beam π's provided a reference signal at about 63 MeV and phototube linearity was found to be adequate up to 200 MeV (from protons which just stopped in the counter). The threshold was estimated to correspond to a proton of energy 14 ± 2 MeV. The total pulse amplitude from the six counters was also recorded.

The estimate of the efficiency of the counters was based on the measurements below 130 MeV of Crabb *et al.*[10] on almost identical counters and their extrapolation of the calculation of Kurz[11] up to higher energies. The timing resolution was determined from a study of fast π's, fast protons and neutrons from backward elastic and charge exchange scattering, and fast neutrons from the reaction $\pi^- + p \rightarrow \eta + n$ at 725 MeV/c. After a final correction for pulse amplitude, for charged particles the standard deviation was 0.5 nsec. For neutrons the resolution was divided into an intrinsic part, having a standard deviation of 0.6 nsec, and a second part, usually small, which was a function of the neutron velocity relative to the velocity of light in the counter and arose from the different possible interaction points inside the counter.

Slow neutral particles detected by the counters were usually assumed to be neutrons although K_L^0 could be present and this possibility was considered in the interpretation of any structure. Likewise slow charged particles could be $\pi^\pm$ or $K^\pm$. The low mass of the π reduces greatly the acceptance of these particles by the counters in the velocity range of interest. Slow protons could be recognized by their characteristic ionization loss

or energy deposited in the neutron counters. No evidence was seen for smaller signals corresponding to $\pi^{\pm}$ or $K^{\pm}$ and typically the contamination from this source was estimated to be < 10%.

Neutrons were usually selected by demanding a pulse in a neutron counter with no pulses detected in any of the 9-mm thick scintillation counters $A1$–6 or in the P counter. Typically about 4% of neutrons activated two counters.

Decay Counters

As the final nucleon was detected in the neutron counters, an arrangement of detectors which merely counted the number of charged particles and γ rays leaving the hydrogen target should suffice to distinguish several of the simpler final states. Then from the nature of the missing-mass technique, the mass scale and resolution in all of these decay channels would be identical. The task of separating the final channels was clearly helped by charge conservation. For strong decays of resonances, G parity conservation also limited the number of possible final pion states, furthermore for these decays γ rays would usually be produced in pairs.

The arrangement of decay counters used is indicated in Fig. 4. Charged particles were detected primarily by 20 counters, $C1$–20, each of which consisted of two strips of scintillator in the form of an "L." The downstream, or "lid" end of the counter had an 18° taper. The two halves were cemented together and viewed by a single photomultiplier via an air and aluminum foil light guide to avoid Čerenkov light from γ cascades. Behind each arm of the "L" was a separate γ detector. Each of these 40 counters consisted of six layers of lead, each 0.7 radiation lengths thick and six layers of scintillator. In addition to γ detection they served to divide into two regions the polar angular range subtended by the charged particle counters. Further subdivision at forward angles was effected by two pairs of counters $R1,R2$ and $K1,K2$. The upstream end of the cylinder was nearly closed by two semicircular counters $D1$ and $D2$.

The efficiency of the γ counters was determined over a range of energies and angles from 30 to 1500 MeV in a subsidiary experiment. Electrons of the required energy entered a 0.1 radiation-length copper converter and events were selected in which no charged particle emerged with more than a few MeV. This simple form of "tagging" was found to be very satisfactory. Otherwise the main tests of the system were performed using the nonresonant channels $\pi^-\pi^0 p$ and $\pi^+\pi^- n$ and the decay $\eta \rightarrow 2\gamma$. As an example of the technique

consider events with one charged π and two γ's in the decay counters. The 2γ's are predicted and usually found to be close together and opposite the π. This was used to study the behavior of π's, for example it was found that about 5% of π's had a signal in the adjacent γ counter in addition to the one directly behind the charged particle counter. A study of the $\eta \rightarrow 2\gamma$ decay confirmed the measured efficiencies of the γ counters but also showed that in some 10% of the cases when a γ was detected the corresponding charged counter also fired. Only about half of this was understood in terms of pair production in the hydrogen target and walls etc. The remainder was attributed to the detection of Compton electrons from very low-energy photons from the shower.[12] A comparable number of events were also seen in which a different charged counter fired and this could also be understood by such a process.

Information from such studies together with the earlier results on γ-counter efficiencies and the geometry of the apparatus was incorporated into a Monte Carlo program to simulate meson decay. Predicted and measured efficiencies could be compared for $\omega \rightarrow \pi^+\pi^-\pi^0$, and this comparison was used as a basis for estimating the magnitude of the errors in the simulation program. Qualitatively the efficiencies were in broad agreement and while some observed decay configurations had no counterpart in the simulation program, in general agreement was observed, to about ±10% to ±20% of the efficiency, in the main decay configurations.[12]

Electronics

Essentially the experiment consisted of measurements of the ratio of neutrons detected within a particular time-of-flight gate to the number of incident beam pions as a function of beam momentum P_1. A wide mass coverage implied data collection over many momentum bins and consequently at different times. Thus the over-all reproducibility of the apparatus was of particular importance. The two main problems were the general stability and the reproducibility under varying conditions of beam intensity and duty cycle.

All beam particles of the same momentum counted by the beam scalers, should have the same probability of producing a given type of event. It was this probability, or cross section, whose variation with momentum was to be measured. In all the counters in the experiment, most of the pulses were produced by particles originally in or close to the beam. The large collimators near H (Fig. 5) meant that almost all such parti-

cles had to pass through S or V. Consequently, rejection of events in which a second particle was detected by one of these counters ensured that as far as possible beam particles were only counted if the rest of the apparatus was able to record accurately an event.

Coincidences were made between each of the hodoscope counters and the timing counter S (resolving time about 15 nsec). The required combinations of hodoscope counters were then selected and combined to form the five momentum channels. Subsidiary circuits checked that only one G hodoscope counter pulse and similarly only one H pulse were present, that the particle was not an electron, that there was no stray beam particle in V and no other pulse in S within 40 nsec. If all these conditions were satisfied the pulse was counted in the appropriate beam scaler and a signal signifying a good beam particle produced.

In addition to the constancy of the threshold energy in the neutron counters two factors were important in the measurement of the number of neutrons in a given time-of-flight gate. Almost all detected neutrons produced a pulse, within a wide amplitude range, in one neutron counter only and there was no clear way to distinguish genuine events from those in which a stray pulse in a counter was in accidental coincidence with an interacting beam particle. The number of such events was measured in a region too early to be accessible to beam induced triggers, but the problem remained that the effective background rate in the neutron counters could be strongly time-dependent. For example, if some of the counts were produced by particles which also initiated pulses in other counters, then readout, veto or coincidence resolving times for these counters could lead to structure in the time-of-flight spectrum. Care was taken to minimize such effects but ultimately reliance had to be placed on the consistency of the data. They could be particularly serious if data were accumulated at one beam momentum only.

The second factor was that resonances had to be seen against the nonresonant background, which as already noted falls very rapidly with increasing time of flight. This made the measured rate sensitive to the width and particularly the position of the neutron time-of-flight gate used in the data analysis. This gate was typically 5-nsec wide and in a region such that a change in position of 1 nsec led to a change of about 10% in the rate. This was always important, but was particularly serious at the X^0. Most sources of variation were ultimately associated with changes in temperatures. All critical elements, the photomultiplers

in S and $N1$–6, the discriminator and coincidence electronics, the digitizers, and certain voltage supplies, were kept in temperature-controlled enclosures, typically stable to $\pm 1\,°C$.

The six neutron counter outputs were combined to produce a single pulse train. A long dead time (120 nsec) introduced at this point meant that if more than one pulse were present in the counters, only the first was considered by the coincidence electronics. This requirement reduced certain backgrounds but did imply that if a fast secondary particle entered the neutron counters no slow neutron or proton could be detected. In normal operation three final coincidence gates were used; all of these were opened by a neutron pulse. Noninteracting beam particles were vetoed by counters $V1$ or $V2$. Otherwise, beam pulses entered the gates and if any were open at the appropriate time, produced a final coincidence. This caused the state of all counters in the system to be read into a store (resolving time -20 to $+40$ nsec), the computer to be flagged, a time-of-flight digitizer to be activated and the neutron-counter pulse height and the P-counter pulse height to be recorded.

Fast beam π's scattered into the neutron counters provided a reference time, the "fast peak," and one of the three coincidence gates accepted a sample of such events. A second gate responded to neutrons within from 3 to 45 nsec after the fast peak. The third, the "accidentals gate" was set for neutron-counter pulses between 5 and 15 nsec before the fast peak. Typical time-of-flight spectra for protons, i.e., triggers in which the appropriate $A1$–6 has also fired, and neutrons, are shown in Fig. 6. No decay selection has been used. Note the characteristic falling shape of the time-of-flight spectra, the use of the fast peak in "protons" to define zero time and the level of accidental backgrounds. The time of flight of the neutron was digitized in bins of about $\frac{1}{4}$ nsec, the timing scale being calibrated regularly relative to a 100-MHz stabilized crystal oscillator. Timing marks spaced at 10 nsec intervals along the time-of-flight spectrum were generated by stopping and starting the clock at random but in phase with the 100-MHz oscillator in the method described by Baker *et al.*[13] The linearity was checked with a noise generator. The position of the "fast peak" was usually determined to ± 0.02 nsec. However due to the depth of the counters and also the wide range of neutron-pulse amplitudes, there remained a systematic uncertainty in the absolute time of flight of up to 0.5 nsec.

Noise in other counters could have been important, in particular pulses in beam veto counters $V1$ and $V2$ would have rejected good events. How-
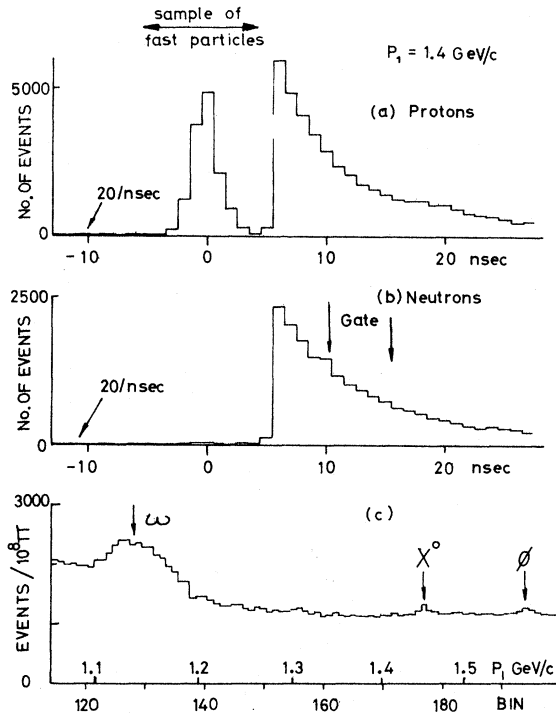
FIG. 6. Typical time-of-flight spectra for (a) charged and (b) neutral particles at 1.4 GeV/c. Both spectra fall rapidly with increasing time. A sample of fast particles (mainly scattered π mesons from the beam), monitors time zero. The accidental coincidence rate is measured at negative times. It is barely visible and the average level is as indicated. The time scale shown is approximate only. (c) shows the number of neutrons within the gate indicated in (b) as a function of incident momentum. The X^0 and ϕ can be seen on an almost constant background. The gate used is in the threshold region for the X^0 and ϕ but well above threshold for the ω, which is consequently detected over a wide range of momenta.

ever, almost all pulses in these counters were produced by beam particles and were therefore discounted by vetoes in S and V referred to above. The residual "occupancy" was monitored but was usually less than 1%. Noise in the decay-counter system moved events from one class into another but this effect was again small.

Data Collection and Reduction

A beam intensity of 2×10^5 π's produced about 110 triggers/burst. For each of these triggers, sixteen 12-bit words were read into the memory of a *PDP*8 computer in about 60 μsec using the data break facility and stored on a magnetic disk.

At the end of each burst the data were recovered from the disk, analyzed and together with addi-

tional scalers giving the number of beam particles in each of the five momentum channels and other monitor information, written on seven track magnetic tape. A complete tape or run represented about 6×10^8 incident pions.

All the scalers were set to zero before each burst so that if an error were detected the entire burst could be rejected. No individual events were rejected on-line. Histograms of counter distributions, pulse height and time-of-flight spectra and various monitor rates were accumulated on the disk, examined at the end of each run, and important rates monitored as the experiment progressed.

The main stage in the "off-line" analysis involved the creation of data summary tapes consisting of sets of up to 90 time-of-flight spectra, with five such sets for each run, corresponding to the five momenta. An event was first checked for consistency with the requirements of the electronic selection and interface electronics. The fraction rejected from all such sources was nearly always less than 1%. The digitized time of flight was corrected for pulse-height variation, redefined in terms of a zero based on the position of the fast peak and recast into double bins, each about 0.5-nsec long. Finally the event was checked against the requirements for a neutron or a proton, the decay configuration likewise examined, and the event allotted to the appropriate time-of-flight spectrum.

IV. EXTRACTION OF RESONANCE PARAMETERS

From the data we can obtain the behavior of $(d^2\sigma/dtdM_3)_{\theta 4}$ as a function of say t and M_3. The general assumption made in the analysis is that this can be interpreted in terms of narrow Breit-Wigner resonances superimposed on an incoherent and slowly varying background. We have seen that at a given time-of-flight τ the Jacobian J_τ [Eq. (6)] connecting the counting rate and the cross section also varies only slowly with P_1. In Fig. 6(c) is shown the counting rate as a function of P_1 for events in the time-of-flight gate from 10 to 15 nsec. The background level above the ω is remarkably constant. Over the small mass range usually required, a linear or at most a quadratic parameterization of the background should be adequate. The assumption of incoherence indicates a limitation in the technique and implies that consideration may have to be given to interference effects in the final interpretation.

The general expression for the number of detected neutrons can be obtained by combining Eqs. (5) and (7). This gives

$$N = \frac{N_H}{2\pi} \int_{\Delta\Omega} \int_{\Delta\tau} \int_{\Delta P_1} d\Omega d\tau dP_1$$

$$\times \frac{\Gamma/2\pi}{(M_3 - M_0)^2 + \frac{1}{4}\Gamma^2} J_\tau \frac{d\sigma}{dt} n(P_1) \eta(\tau).$$

$$(9)$$

The factor $n(P_1)$ is the momentum distribution of the incident beam either at one momentum setting or over a range of momentum bins. This distribution should describe the momentum at the interaction, i.e., after allowance for ionization loss in the target. $\eta(\tau)$ represents the neutron-counter efficiency.

Suppose firstly that the ranges $\Delta\Omega$, $\Delta\tau$, and ΔP_1 are sufficiently narrow for the resultant variation in M_3 to be $\ll \frac{1}{2}\Gamma$. Then in view of the almost linear relationship between M_3 and P_1, the number of events detected, normalized to the incident pions as P_1 is varied, will follow the Breit-Wigner shape at all τ. Notice that there is no explicit reference to the threshold momentum and the behavior is continuous across the threshold region. Notice also that this is independent of the neutron-counter efficiency and the t dependence of the cross section. If the restriction is now relaxed and the actual ranges of the variables is used, the Breit-Wigner form will be modified by the experimental resolution. The shape will then depend on the value of τ chosen. Otherwise the conclusions will be unaltered apart from the effect of errors in τ which make the behavior at a given, measured value of τ somewhat dependent on the cross section and neutron-counter efficiency at nearby values. The nonlinearities near threshold and the various minor effects additional to those treated here resulted in our using Monte Carlo techniques to extract the best values of the mass and width. These will be described later. However (9) can be carried a stage further to demonstrate the extraction of the cross-section information.

For given τ and θ_4, P_1 can be treated as a function of M_3 through Eq. (1) and an integral over a wide range of P_1 replaced by a corresponding integral in M_3 over the resonance. Using the values at M_0 for those quantities which are almost independent of P_1 or M_3, and noting that the Breit-Wigner expression is normalized, the integral over M_3 gives

$$N = \frac{N_H}{2\pi} \int_{\Delta\Omega} \int_{\Delta\tau} d\Omega d\tau \, J_\tau \frac{d\sigma}{dt} \frac{\partial P_1}{\partial M_3} n(M_0) \eta(\tau).$$

This can be further simplified as neither J_τ nor $\partial P_1 / \partial M_3$ vary significantly over the small range of θ_4 in the experiment:

$$N = \frac{N_H}{2\pi} \Delta\Omega \frac{\partial P_1}{\partial M_3} (M_0) n(M_0) \int_{\Delta\tau} d\tau \, \eta(\tau) J_\tau \frac{d\sigma}{dt}. \quad (10)$$

As the time of flight is a function of t only, this integral gives directly an average value of $d\sigma/dt$ in a given t interval.

The description in terms of $d\sigma/dt$ points to a sensitive way to examine the cross section down to very low values of the final-state c.m. momentum P^*. In Part II it was shown that the simple S-wave behavior, characterized by a total cross section rising linearly with P^* and an isotropic angular distribution, was equivalent to a $d\sigma/dt$ independent of both P^* and the c.m. angle θ_4^*. If this situation obtains, then a plot of $d\sigma/dt$ against t should show a constant value, with no discontinuity through the resonance in spite of the rapid variation in P^*. In Fig. 7 is shown the type of variation in $d\sigma/dt$ that might be expected, under various assumptions, in the limiting case of a point neutron counter at $0°$. Thus although P_1 is allowed to vary, whereas a cross section is usually defined for P_1 fixed, the description (7) and its incorporation in (10) avoid a correction for the kinematic factors which distort a resonance very close to threshold.

To assist in the determination of resonance parameters and cross sections, a Monte Carlo simulation of the production process was used. The main effects considered were the momentum profile within a momentum bin, the mean ionization loss in the beam counters and hydrogen target, the range of neutron angles accepted and the time-of-
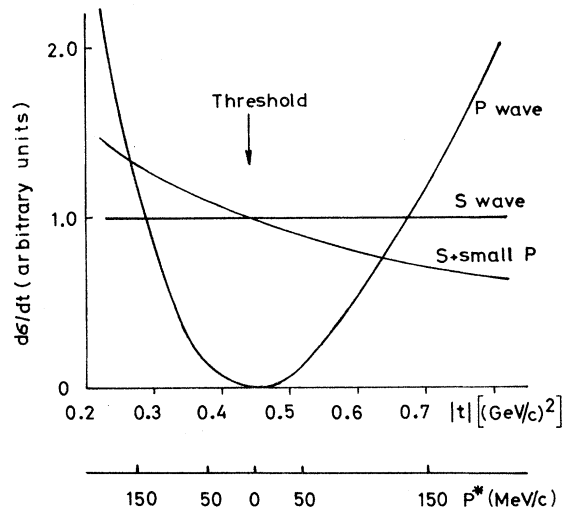

FIG. 7. Predicted behavior of $d\sigma/dt$ as a function of t just above the threshold in the reaction $\pi^- + p \to X^0(985) + n$ for various angular momenta in the final state when the neutron is detected at zero degrees. Note also the P^* scale.

flight error. Minor effects included the range of incident beam angles, the predicted aberrations in the momentum spectrometer , and Landau fluctuations in the ionization loss in and before the target. The simple Breit-Wigner form of the resonance together with a linear rise in its cross section as a function of $P*$ was assumed. The program was used to generate time-of-flight spectra over the required range of momentum bins. These spectra could then be analyzed in the same way as the data and comparisons made at any stage. Thus in the extraction of the cross section behavior, the data were fitted with the appropriate polynomial to describe the background together with the predicted signal from the Monte Carlo simulation. Apart from minor corrections, the relative normalization then gave the measured value of $d\sigma/dt$.

The highest mass resolution and the lowest error in the absolute mass are available closest to the threshold. As outlined in Sec. II the mass and width information lay in the measurement of the relative number of events detected in a fixed time-of-flight gate as P_1 was scanned through the mass range. For a narrow resonance the choice of the gate width was usually made according to the following procedure. The approximate resonance parameters were first determined and were then incorporated in a Monte Carlo simulation which generated time-of-flight spectra across the threshold region. These were then inspected to find the widest gate possible subject to the constraint that an error of up to 0.5 nsec in its absolute position would have a negligible effect on the predicted yield of neutrons. This allowed for possible errors in the absolute time-of-flight scale for measured neutrons. Optimization of the signal/background ratio would usually produce a somewhat wider gate. The choice was a slow function of the resonance mass and width.

The decay system could also be used to make a selection of the events, either to emphasize a particular channel or to increase the statistical accuracy of the measurements by reducing certain backgrounds. Clearly, for the cross-section determinations, minimum selection is to be preferred in order to avoid an additional uncertainty in the results. Generally the detailed decisions as to which decay configurations should be included were made by comparing the predicted signal from the resonance (assuming the decay branching ratios) with the measured background below threshold. Given a set of such comparisons for the various configurations the choice could be made according to the appropriate criteria. With the possible exception of the K^+K^- channel in the study of the ϕ, the variation in the efficiency of

the decay selection with P_1 should have a negligible effect on the measured number of neutrons.

The experimental data within the selected time-of-flight gate were directly compared to Monte Carlo predictions which assumed different masses and widths, and χ^2 calculated in each case. For the relatively wide ω we allowed a low-order polynomial background; for the η, X^0, and ϕ a a straight line sufficed.

Statistical errors on the mass and width were generally determined by noting where χ^2 increased by 1 from its minimum value.

Apart from the statistical error, the only significant contribution to the error in the absolute mass arose from the uncertainty in the absolute beam momentum discussed in Sec. III. In view of the results obtained with the floating wire calibration this was described by a standard deviation of 0.08% of P_1.

Some insight into the basis and accuracy of the width determination can be gained by examining the behavior predicted in the threshold region for a fixed mass of resonance as the width is varied. This is shown in Fig. 8 for $M_0 = 958$ MeV. Inte-
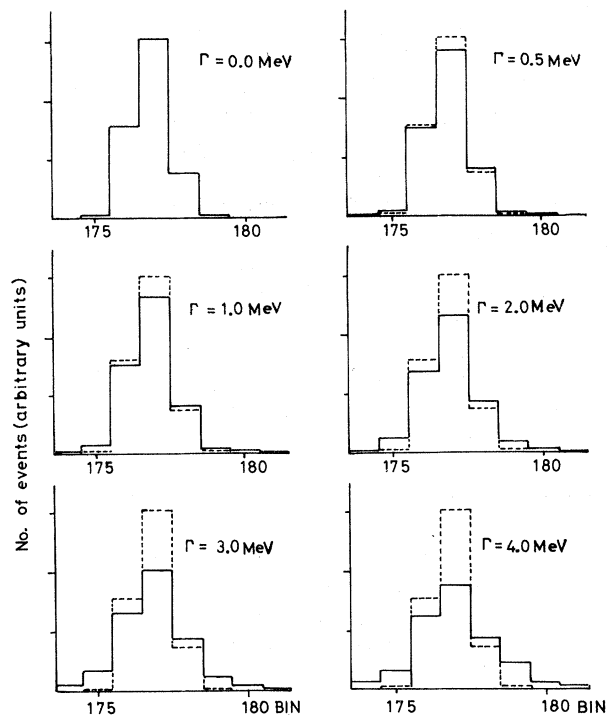

FIG. 8. Predicted behavior of the distribution of neutrons across the X^0 threshold with beam momentum as a function of the assumed width. The dashed lines are drawn for $\Gamma = 0.0$ MeV. While the total number of events remains almost constant, for small Γ the number in the central bin falls almost linearly with Γ. The lost events reappear in the tails.

grated over P_1 the total number of events is al-
most independent of the width—as required by
(10). However the number of events in the central
momentum bin falls almost linearly as Γ in-
creases, even for $\Gamma < 1$ MeV. The bin spacing at
this mass is equivalent to about 3.5 MeV and,
mainly as a result of the length of the hydrogen
target, each bin covers a range in M_3 with a
f.w.h.m. of about 5 MeV. The effect arises largely
from the general form of a Breit-Wigner reso-
nance, in which the fraction outside the limits
$M_0 \pm \Delta M$ is approximately $\Gamma/(\pi \Delta M)$ for $\Delta M \gg \frac{1}{2}\Gamma$.
As only narrow resonances are being discussed,
this is probably reliable. The loss of events from
the central bin also increases the width of the
distribution.

The possible sources of error in the determina-
tion of $d\sigma/dt$ are statistics, assumptions about
background behavior, uncertainty in the neutron-
counter efficiency and in absolute time-of-flight
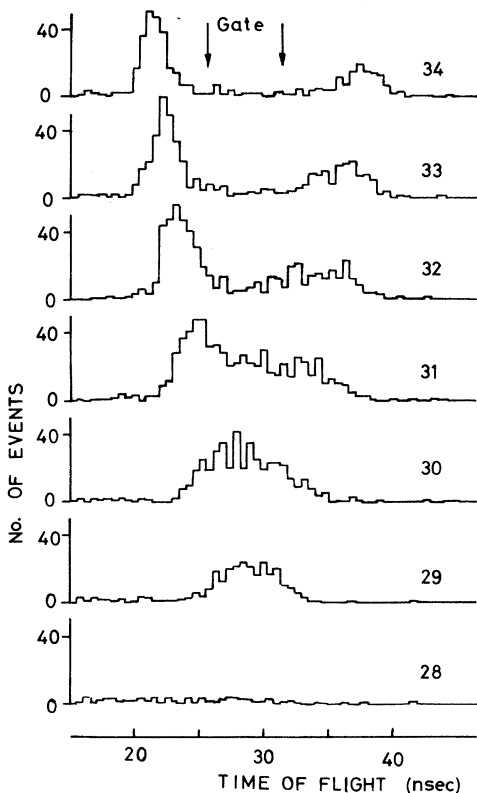scale. The relative importance of these depended

on the resonance studied and further discussion
is delayed until Sec. V.

V. RESULTS

In this section we present the results obtained
from a study of the four mesons η, ω, X^0, and ϕ
and also some evidence of structure in the $\pi^+\pi^-$
channel at the threshold for two charged K's. The
most extensive data were collected in the region
of the X^0, but shorter runs were made down to
below the threshold for ω production and a sepa-
rate set of three short runs across the η threshold.

The η Meson

The lifetime of the η has been determined by
means of the Primakoff effect[14] and is sufficiently
long for the width to be neglected in this experi-
ment. The cross section has been shown to be
large and dominated by an S-wave behavior.[6] The
2γ decay offered an almost background free selec-
tion of η's. The main interests lay in the detailed
behavior of the cross section and in the possibility
of checking and investigating the mass resolution.

Limited data comprising about 6×10^7 incident
π's/momentum bin were obtained from three runs
covering in all 15 bins from 679.7 MeV/c (bin 26)
to 728.8 MeV/c. Figure 9 shows time-of-flight
spectra for events with a 2γ selection. The re-
sidual background presumably consists mainly of
nonresonant $2\pi^0$ production.

A time-of-flight cut, or gate, from 25.6 to 31.4
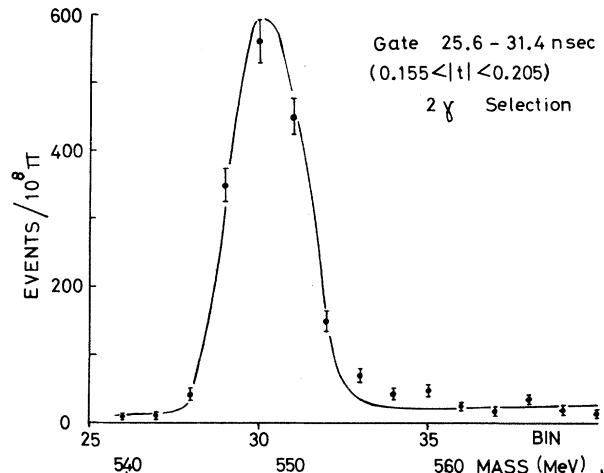nsec was chosen. Figure 10 shows the number of

FIG. 9. Time-of-flight spectra obtained close to the
η threshold at a series of momenta spaced at 0.5% in-
tervals from bin 28 (686.5 MeV/c) to bin 34 (707.3
MeV/c). A selection for two coplanar γ rays has been
made and this gives an almost background-free signal.
The time-of-flight gate used in the extraction of the
mass and width is also shown.

FIG. 10. The number of neutrons within the gate
shown in Fig. 9, normalized to 10^8 incident beam par-
ticles and subject to the same 2γ selection, as a func-
tion of beam momentum. The solid line shows the pre-
diction for a mass of 548.1 and a width of zero. A
linear background has been allowed. A small but
significant discrepancy is noted from bins 33 to 35.

neutrons detected in this gate as a function of momentum. The 2γ selection has again been applied. The gate position is also indicated in Fig. 9. The distribution was fitted with a straight line background plus a set of Monte Carlo predictions as described in Part IV. The χ^2 distribution as a function of mass gave a sharp minimum at 548.1 ± 0.1 MeV. After allowing for the uncertainty in the absolute momentum the value for the mass is 548.1 ± 0.4 MeV.

Figure 10 shows the yield in the gate as a function of momentum along with the Monte Carlo prediction for a width of zero. Agreement is good apart from a small discrepancy at the higher mass side of the resonance. In this region very many η's are produced and the associated neutrons only avoid being detected because they arrive at the wrong time or because they are outside the angular acceptance. We interpret the extra events as being principally due to rescattering of up to 0.5% of the produced neutrons back into the neutron counters from the supporting framework and shielding. Because of these extra events at the high mass side, the best fit to the data as a function of the width was obtained for $\Gamma = 0.6$ MeV. The fit however was poor, with $\chi^2 = 34$ for 12 degrees of freedom.

It is interesting to compare these results with the earlier work of Jones et $al.$[6] in which the width was found to be less than 0.9 MeV [95% confidence level (C.L.)]. The technique was basically similar, except that the total number of η's detected was measured as a function of beam momentum and attention was concentrated on the rising edge. This approach was probably preferable for the η but less satisfactory for the study of other mesons where the cross sections are smaller, as it required either a much wider time-of-flight gate, with a consequent increase in the background rates, or the prior subtraction of the background at each momentum which would introduce additional uncertainties. But problems encountered here on the high-mass side of the resonance would be largely absent.

Values for $d\sigma/dt$ as a function of t were extracted by the method described in Part IV. The relatively low mass of the η together with the limited range of momenta at which data were collected meant that all measurements were confined to nine values of t from -0.12 to -0.28 $(\text{GeV}/c)^2$. To avoid normalization errors no decay selection was used. Typical distributions, both for data and the Monte Carlo simulation, are shown in Fig. 11(a) and 11(b). General agreement is good. An uncertainty in $d\sigma/dt$ arose from the estimated neutron-counter efficiency; this estimate was particularly sensitive to the discrimi-

nator bias at the lowest t.

The results for $d\sigma/dt$ at the η are summarized in Fig. 11(c). This figure also shows the mean value of P^* for the various intervals of t. Closest to threshold the value of $d\sigma/dt$ corresponds to a rise of cross section at a rate of $\sigma/P^* = 21.2$ ± 1.8 μb/(MeV/c). We have recalculated the value of Jones et $al.$ [$\sigma/P^* = 17.0 \pm 2.3$ μb/(MeV/c)] using more recent values of the $\eta \rightarrow$ neutrals branching ratio and the neutron-counter efficiency[10] and find 22 ± 3 μb/(MeV/c) in good agreement with the present result. It is interesting that at $t = -0.18$ the η's must have been produced by beam π's having a momentum of about 1 MeV/c above the reaction threshold.

Above threshold, at lower and higher t, the results indicate an increasing P-wave contribution to the final state, characterized by an increasing forward/backward asymmetry. Such a
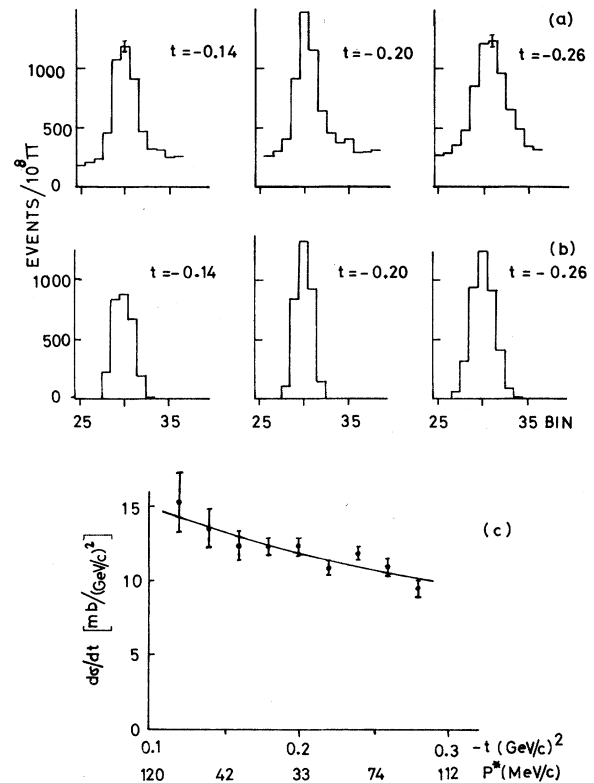

FIG. 11. Typical mass spectra at the η (a) are compared with the corresponding Monte Carlo predictions for an S-wave cross section (b). No decay selection has been used. An apparent small shift in the mass at $t = -0.26$ $(\text{GeV}/c)^2$ is attributed to an error of about 0.3 nsec in the absolute time-of-flight scale in this region. (c) $d\sigma/dt$ for the η as a function of t. The behavior is mainly S wave, with evidence for some P wave also. The corresponding c.m. momentum P^* of the η is indicated.

P-wave term would be consistent with the results of Buniatov *et al.*[15] at 718 MeV/*c* and not inconsistent with those of Jones *et al.*[6] and Richards *et al.*[16] To quantify the result, the present data were fitted with a combination of *S* and *P* waves. The small angle between the detected neutrons and the beam direction means that the transverse momentum is always small, ≈ 30 MeV/*c*. In this circumstance it is reasonable to neglect the *P*-wave spin-flip amplitude. The cross section should therefore be of the form

$$\frac{d\sigma}{dt} \propto |\ 1 + \beta P^* \cos\theta^* e^{i\delta}\ |^2\ ,$$

where β and δ are real and are a measure of the relative *P*- to *S*-wave contribution. Figure 11(c) shows the best fit, which was obtained with the values $\beta\cos\delta = (-9 \pm 3) \times 10^{-4}$ (MeV/*c*)$^{-1}$ and $\beta^2 = (-4 \pm 9) \times 10^{-6}$ (MeV/*c*)$^{-2}$.

The ω Meson

The ω meson has been studied in many experiments and its main properties are well known. Most of the decay proceeds via the $\pi^+\pi^-\pi^0$ channel and is therefore readily identified in the decay array. The cross section near threshold is found to be relatively high. The width of about 10 MeV is appreciably greater than the mass resolution available in this experiment which is about 4.5-MeV f.w.h.m. in the threshold-crossing region. We report on the detailed behavior of the cross section close to threshold and also give values for the mass and the width.

Data were available at all momenta of interest from well below threshold. Runs were spaced at intervals of $2\frac{1}{2}\%$ in P_1 so that there was one contribution of about 10^8 incident π's in each momentum bin.

The mass and the width were determined using events for which two charged particles and two γ rays were detected. The time-of-flight gate chosen lay between 16.1 and 20.9 nsec. Figure 12

shows the yield of neutrons as a function of beam momentum. This was fitted between bins 96 and 158 with a second-order polynomial together with the Monte Carlo prediction. Minimum χ^2 was found at a missing mass of 782.3 ± 0.4 Mev. ($\chi^2 = 72$ for 59 degrees of freedom.) A linear background gave a similar result. After allowing for the uncertainty in the absolute momentum this gave a final value of the mass of 782.3 ± 0.6 MeV. The width was found to be 12.4 ± 2.2 MeV, the error being statistical. The use of a linear rather than a quadratic background increased this by about 0.2 MeV.

To investigate the cross section near threshold the yield of ω's was determined in ten adjacent intervals of t. Figure 13 shows typical mass plots. To avoid uncertainties in the efficiency of any decay selection procedure, all neutron events have been included. The background is consequently relatively high. Third- and fourth-order polynomials were used and gave essentially identical results. After small corrections for possible errors in the absolute time of flight scale, satisfactory fits were obtained at all values of t.

The results for $d\sigma/dt$ are summarized in Fig. 14(a). They show a depression of $d\sigma/dt$ close to threshold ($P^* < 80$ MeV/*c*). It seems unlikely that this could be an *s*-channel effect, as in terms of the total c.m. energy the rapid variation occurs over a range of mass from 1724 to 1734 MeV with little further variation up to 1770 MeV. There is no significant forward/backward asymmetry up to at least $P^* = 140$ MeV/*c*. From a
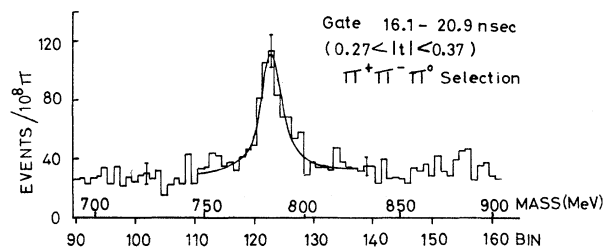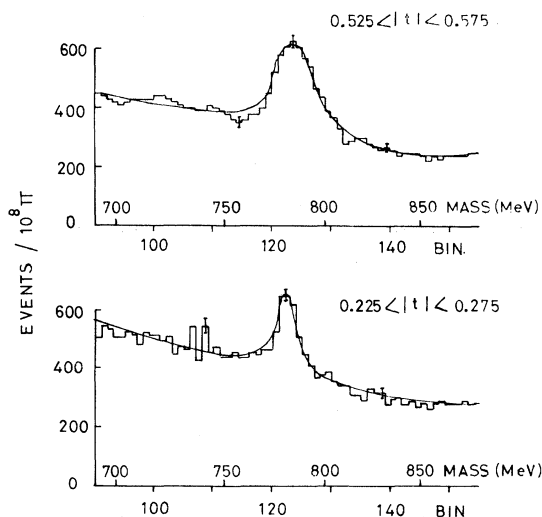

FIG. 12. Threshold crossing at the ω. A selection for the $\pi^+\pi^-\pi^0$ decay mode has been made and the number of neutrons within a time-of-flight gate from 16.1 to 20.9 nsec is shown as a function of beam momentum. The best fit to the data is also shown.

FIG. 13. Typical mass spectra around the ω from which values of $d\sigma/dt$ are extracted. The curves show the fitted distributions. No decay selection has been used. At high t, where $\partial M_3/\partial\tau$ is large, statistical errors are correlated over several mass bins.
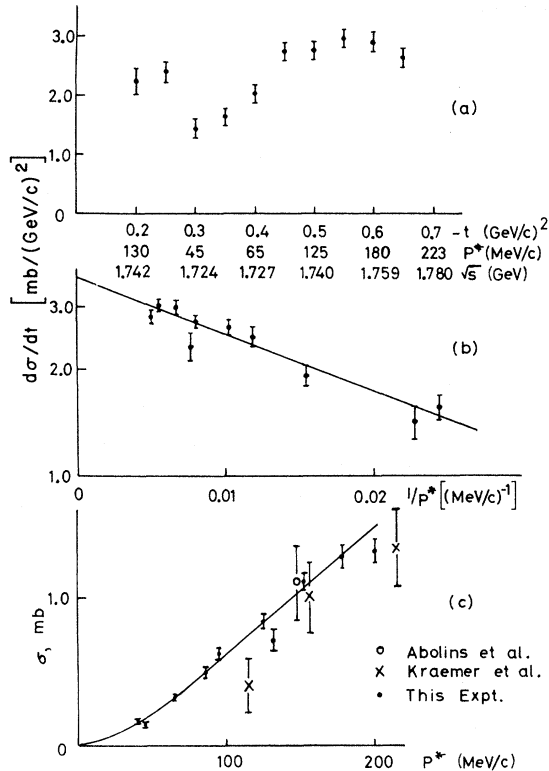
FIG. 14. (a) The cross section $d\sigma/dt$ for the ω as a function of t. $d\sigma/dt$ appears to be a function of P^*, with its smallest value at the minimum of P^*. (b) The same data replotted, on a logarithmic scale, to allow comparison with a simple model in which $d\sigma/dt$ is constant at production but ω's decaying within a distance R from the neutron are removed through a final-state interaction. The straight line corresponds to $R = 1.5$ F. (c) Total cross section plotted against P^* assuming an isotropic production cross section. The smooth curve is based on the simple model described in (b).

study of $\pi^+ + n \to \omega + p$ at a c.m. energy below 1.8 GeV, $P^* \leqslant 260$ MeV/c, Abolins *et al.*[17] also report an isotropic production angular distribution indicative of an S wave in the ω-nucleon system.

Because of the short life of the ω a possible interpretation is that the depressed production close to threshold is the result of a final-state interaction between the neutron and the ω decay products. In the decay $\omega \to \pi^+\pi^-\pi^0$ the pions have an average momentum of about 220 MeV/c in the ω rest frame, which at threshold coincides with that of the neutron. This momentum is near the maximum of the πN scattering cross section and therefore the probability of at least one of the decay pions interacting with the neutron is high.

In Fig. 14(b) we show $d\sigma/dt$ on a logarithmic scale plotted against $1/P^*$. The straight line fitted to the data is based on a simple model in

which we assume

(a) production of ω's occurs with an S wave between the ω and neutron;

(b) there is an effective distance R such that ω's decaying within R from the neutron are removed; those outside R are unaffected.

For a width $\Gamma_\omega = 10$ MeV these assumptions imply a variation of $d\sigma/dt$ with P^* of the form $d\sigma/dt \propto \exp(-22R/P^*c)$, where R is measured in fermis. The fit to the data corresponds to $R = 1.5$F, which is reasonable. From the S-wave assumption the measured $d\sigma/dt$ at various P^* can be converted into an equivalent total cross section. This is shown in Fig. 14(c) together with the fit and the results from other experiments.[17,18] The model implies that the true S-wave production cross section $d\sigma/dt$ at threshold is about 3.5 mb/(GeV/c)^2 [Fig. 14(b)].

The explanation advanced would suggest a difference in the behavior in the $\pi^0\gamma$ and 3π channels. Alternatively, if for example the production mechanism only were responsible, the effect would be seen equally in both. The present statistical accuracy is inadequate for this check to be made. Assuming, however, that the explanation is basically correct, the ω behavior allows an estimate to be made of the effect of a final-state interaction on the other cross sections, in particular the X^0 and ϕ. The effect on the measured width of the ω appears to be small.

It is interesting to note that if the linear rise were maintained the cross section for ω production would saturate the $I = \frac{1}{2}$, S-wave πN inelasticity at a P^* near 250 MeV/c. In the case of η production a similar behavior of the cross section was successfully interpreted as being due to the presence just above the ηN threshold of an S_{11} resonance with a large ηN coupling.[19] For ω production an S-wave final state can come either from an S_{11} or a D_{13} πN state whereas for η production only S_{11} is allowed. Also a simple two-channel analysis as applied to η production is probably inadequate at the ω threshold due to the presence of other important channels ($\pi\Delta, \rho N, \eta N$). However it would be surprising if the sudden opening of the ωN channel with such a rapidily rising cross section did not show in the elastic phase shifts. In this context we would like to point out that the second S_{11} resonance around 1700 MeV/c^2 is very close to the ωN threshold and that some phase-shift solutions[20] (especially Berkeley, Path 2) show a rapid change in the elasticity of S_{11} in this region.

If, on the other hand, the strong S-wave ω production is due to a D_{13} resonance around 1700 MeV (a state required by the L excitation quark model[21]), then the strong coupling to the ωN channel

may account for the difficulty of observing this state in elastic phase-shift analyses.

Recently Rosner[22] has pointed out that whenever a meson-meson or meson-baryon system is allowed by the quark model to form a resonance it does so for $P^* \approx 350$ MeV/c and $P^* \approx 250$ MeV/c, respectively. In this context we point out that Brandstetter *et al.*[23] have recently reported evidence for a D_{13} resonance in K^-p, with a large coupling to $\omega\Lambda$, lying in the range 1920 to 1980 MeV/c^2 which is just above the $\omega\Lambda$ threshold at 1894 MeV/c^2.

In conclusion we suggest that the rapidly rising cross section for ω production near threshold is probably due to the existence of either an S_{11} or a D_{13} resonance with a large coupling to ωN.[24]

The X^0 and ϕ Mesons

We examine now our data in the mass range 920 to 1040 MeV which therefore includes the well-established X^0 and ϕ. A measurement of the X^0 cross sections exists[25] in the same reaction at 1.50 and 1.52 GeV/c ($P^* = 190$ MeV/c). The predominant X^0 decay is through $\pi\pi\eta$; this produces a large number of possible final configurations in the decay apparatus, so that selection is difficult. From other experiments the width is less than 4 MeV (Ref. 26) and 3.8 MeV (Ref. 27) [90% confidence level (C.L.)]. The production at low P^* of the ϕ meson by incident π's was reported by Dahl *et al.*[28] and was shown to have an approximately isotropic production angular distribution. Recently very precise data have come from colliding beam experiments.[29] We took advantage of the large branching ratio into the channel K^+K^-, where in view of the low-Q value the opening angle of the $2K$'s is small, to make a decay selection which greatly enhanced the signal/background ratio.

Possible complications exist in this mass range in that evidence from other experiments for several additional states has been reported. Some doubt has been cast on the uniqueness of the X^0 itself as there is the possibility of a second meson[30] $M(953)$ with rather similar decay modes. The two narrow states recently reported[31] in the reaction $\pi^- + p \rightarrow x^0 + n$ at an incident momentum of 2.4 GeV/c have masses of 940.1 ± 1.6 and 962.5 ± 1.6 MeV. The latter could be the neutral counterpart of the original narrow $\delta^-(962)$.[32] Relatively wide states may also be present,[33] in particular the $\pi_N(980)$, $\Gamma \approx 60$ MeV. Also there is evidence for a pole, the S^*, in the S-wave $\pi\pi$ scattering amplitude at a mass of 980 MeV.[34]

Some of the analysis of our data has already been published.[1] It was found that the cross sections for X^0 and ϕ production are small, with values of σ/P^* near threshold only a few percent of those obtaining for the η and ω. There was no evidence for any peaks at 940 or 962 MeV, which would imply cross sections for these mesons much less than the X^0 in contrast with the original experiment of Cheshire *et al.*[31] where the cross sections were reported to be greater. We determined the X^0 mass to be 957.1 ± 0.45 MeV and the width to be less than 1.9 MeV (95% C.L.). The narrow width implied that if the $M(953)$ were also present in the data then the mass difference and both widths would have to be less than about 2 MeV. Using the measured branching ratio for $(X^0 \rightarrow 2\gamma)/(X^0 \rightarrow \text{total})$, the upper limit on the width gave some support for linear mixing in the pseudoscalar-meson nonet. Finally we found the ϕ mass to be 1019.1 ± 0.6 MeV, but without a satisfactory selection for the decay mode $\phi \rightarrow K^+K^-$ no significant value for the ϕ width could be obtained. The present paper continues this analysis. The behavior of the cross sections is investigated over a wider range of t. The results of a study of the ϕ in the K^+K^- decay channel are also reported.

Above bin 161 (1332 MeV/c), data collection runs were made at $\frac{1}{2}$% intervals of P_1. As each run covered five momentum bins, the data at each bin came from five separate runs and corresponded to about 5×10^8 incident π's.

To investigate the cross-section behavior in detail the data were divided into ten intervals of t and missing-mass plots constructed. It was found that in the intervals near threshold the X^0 and ϕ were both clearly visible. However, outside this region and particularly at higher t the X^0 signal appeared to be weak. For the purpose of presentation the data have been recombined into four intervals of t only. The resultant spectra, which use no decay selection, are shown in Fig. 15. As the mass resolution is also a function of t, we show the predicted distributions for S-wave production of the X^0. We assume the value of σ/P^* found in the threshold crossing region. It should be remarked that the high value of $\partial M_3/\partial \tau$ at high t in conjunction with the $\frac{1}{2}$-nsec channel widths used in the time-of-flight distributions again leads to some correlation in the mass spectra over two or three mass bins. The relative errors between adjacent points are therefore not wholly random. The effect is only significant for the highest values of t.

It was noted that some of the spectra seemed to show a drop in the background level near mass bin 185, although the effect is small compared to the total rate. To increase the statistical accuracy, data from a very wide range of t were combined. These are shown in Fig. 16(a). The drop at bin 185 is particularly clear in a selection of two
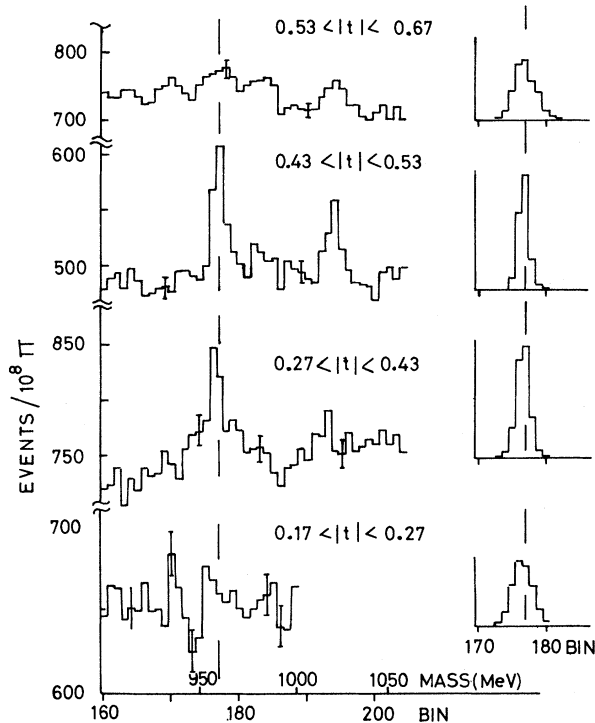
FIG. 15. Mass spectra between about 900 and 1060 MeV for several intervals of t. No decay selection has been used. Note the expanded scales. The X^0 and ϕ both show clearly near threshold. On the right are the X^0 signals predicted for a pure S-wave cross section normalized to the value close to threshold ($t = -0.45$). It appears that $d\sigma/dt$ falls for t both greater and less than this value. There is also some indication of a drop in the background levels near bin 185.
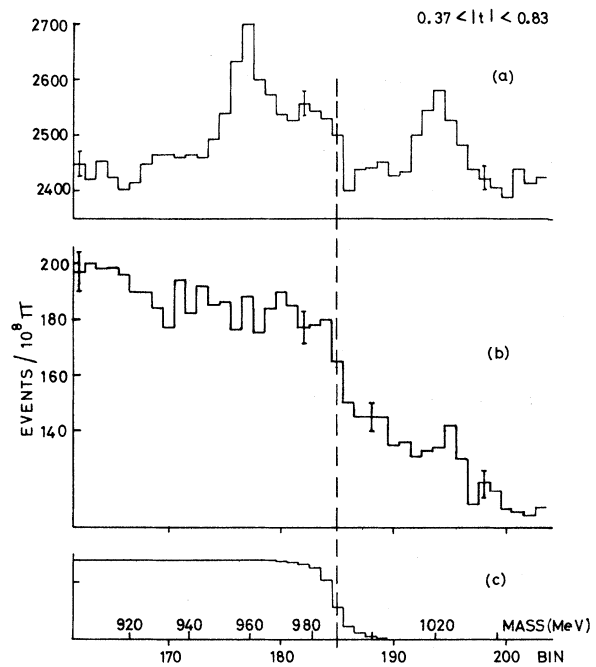

FIG. 16. Mass spectrum for events within a wide range of t. (a) Total neutrons and (b) a $\pi^+\pi^-$ selection. Two charged coplanar particles with an opening angle sufficient to exclude the K^+K^- channel are demanded. A sharp drop is noted near bin 185, particularly in the selected but also in the unselected events. (c) Predicted behavior for a step function at the K^+K^- threshold.

charged particles which are required to have an azimuthal separation of 9 or 10 decay counters, i.e., be nearly coplanar with the beam [Fig. 16(b)]. Such a selection has a high efficiency for the $\pi^+\pi^-$ channel. The K^+K^- channel was excluded by demanding that at least one of the charged particles entered a side γ counter (Fig. 4).

The sharpness of the drop is illustrated in Fig. 16(c), which shows the predicted response to a step function input at a mass of 987.7 MeV, i.e., twice the K^+ mass. As each mass bin is about 3.5-MeV wide, it is clear that the effect is very sharp and that much of it is within a few MeV of the threshold.

A rather similar effect in the 2π mass spectrum has already been reported by Alston-Garnjost et al.[35] and Grayer et al.[36] An analysis of the results of Alston-Garnjost et al. has been made by Flatté et al.[34] by extrapolating the data to the pion pole and describing the behavior in terms of the π-π scattering phase shifts. The S-wave amplitude is dominated by the wide ϵ_0 and the relatively

narrow S^*. The latter couples strongly to the K^+K^- channel. This drop occurs because the phase change across the S^* is superimposed on a background phase of near 90° from the ϵ_0. The 2π amplitude does not however recover above the S^* because of strong absorption by the $2K$ channel.

In order to provide a quantitative estimate of the position of the drop seen in the present data in the 2π spectrum, these were fitted with a step function and a linear background. The range chosen was ± 5 bins around bin 185 (969.4 to 1006.0 MeV). A satisfactory fit was obtained and the best value for the mass at which the drop occured was 989.2 ± 1.5 MeV. This is 1.5 ± 1.5 MeV above the K^+K^- threshold.

The simplest way to explain both the position and the sharpness of the drop is to assume that in the present data the S^* is produced but the ϵ_0 is absent. The problem then reduces to that of the behavior of a resonance at the crossing of the threshold for a new decay channel. This predicts that the $\pi^+\pi^-$ cross section should start to fall exactly at the K^+K^- threshold. The rapidity of the fall is a measure of the relative couplings, g_K and g_π, to the two decay channels. The observed behavior suggests a value of g_K/g_π at least as high as the

figure of 2.5 preferred by Flatté *et al.*[34] The $\pi^+\pi^-$ spectrum below the K^+K^- threshold is not incompatible with the presence of an S^* with a half width of about 37 MeV.

The onset of the K^+K^- threshold effect leads to some difficulty in the determination of the background levels under both the X^0 and the ϕ. For the X^0 an examination of Fig. 16(b) shows however that even for the $\pi^+\pi^-$ channel, in which the drop at bin 185 is most apparent, the variation below this bin is small. We therefore make the usual assumption about the linearity of a backgound over a small range, but keep below the drop itself. The extraction of the mass and width made use of data between bins 172 and 183. Given the deterioration in the resolution at both lower and higher t, a slightly wider range from 167 to 183 was used for the determination of the cross-section behavior. The Monte Carlo simulations (Fig. 15) show that this range should still be adequate.

Information from the decay counters was used in an attempt to reduce the uncertainty in the cross-section measurements. An X^0 decay selection was made by comparing the predicted efficiency for X^0 selection in each of the various possible decay configurations with the background measured in the same configuration just below threshold. The selection was then made of that combination of configurations predicted to give the highest possible X^0 signal in terms of the statistical error. This was the selection previously used in our determination of the X^0 width. The over-all selection efficiency was determined by direct comparison of the data for selected and unselected events in the threshold crossing region and found to be about 75%. Monte Carlo studies showed that the variation of this figure with t was very small. Examples of the resulting spectra are shown in Fig. 17. Expected X^0 signals for an S-wave cross section are again indicated.

The mass spectra, both for the unselected and the selected events, were fitted over a range from mass bin 167 to 183 (924.0 to 980.1 MeV). A linear background was assumed. The cross section we deduced is plotted, after correcting for the selection efficiency, as a function of t in Fig. 18. The same general picture emerges in both cases. It appears that $d\sigma/dt$ has a maximum near threshold (minimum P^*), and there is evidence of a particularly rapid fall at the higher t. The comparison of the data with the S-wave prediction in Fig. 17 shows that while the exact backgound level assumed may be questionable, the relative absence of signal at high t seems clear. The discrepancy is much too large to be accounted for by a variation in neutron-counter efficiency (which should be almost constant in this region) or by an
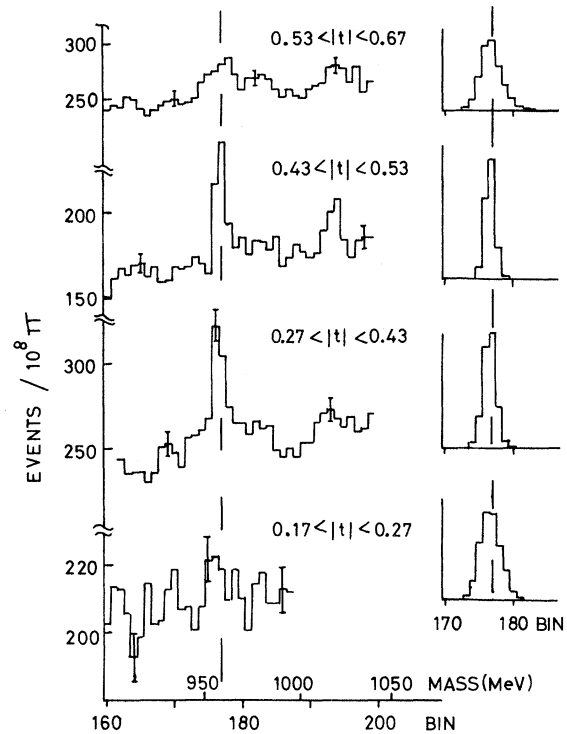

FIG. 17. Mass spectra in the X^0 region in four different t intervals, after making a decay counter selection to enhance the X^0. The corresponding S-wave predictions are shown on the right. Relative to these the X^0 signal is clearly small at both high and low t. Note the reduced background compared with the unselected spectra in Fig. 15.

error in the absolute time-of-flight scale.

We recall that a simple S-wave behavior should yield a constant value for $d\sigma/dt$ while all other waves will give a $d\sigma/dt$ that tends to zero at threshold. The data thus indicates a significant S-wave contribution at threshold and a $d\sigma/dt$ at high and low t which is less than the S-wave contribution. This drop could be produced by interference but an interfering P-wave amplitude would lead to a monotonic rise or fall of $d\sigma/dt$ with t, and so the interference would have to be with a D wave. The presence of significant D waves so close to threshold is, however, surprising.

Since the points at lower and higher t correspond to a slightly higher incident beam momentum, an alternative explanation for their low values could lie in a rapid modulation of the cross section by an s-channel effect such as a narrow N^*. As can be seen in Fig. 18 the rapid fall in $d\sigma/dt$ at high t occurs over a range of $\sqrt{s}$ of only 8 MeV. However, there is no evidence for such a rapid variation on the low-t side where the range of $\sqrt{s}$ is much greater. The measurements of Dufey *et al.*[25] at 1.50 and 1.52 GeV/c give an
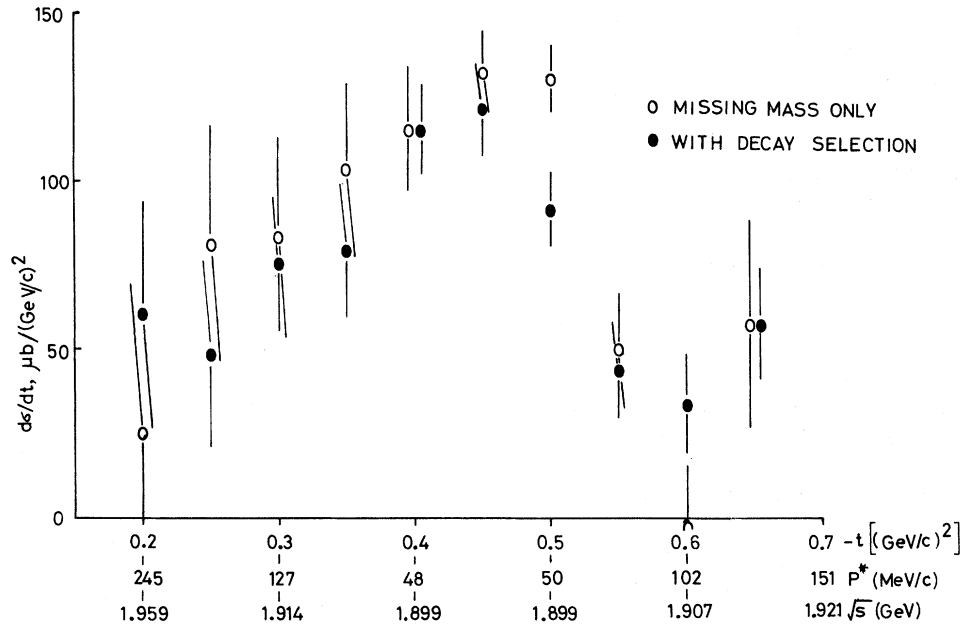
FIG. 18. Values for $d\sigma/dt$ for the X^0. Possible nearby resonances together with the low cross section produce uncertainties in the background subtraction. But the figure shows that similar results are obtained using events with and without decay selection. (See Figs. 15 and 17). In particular, $d\sigma/dt$ passes through a maximum close to threshold.

average value of $d\sigma/dt$ of 130 ± 15 μb/GeV/$c)^2$ at $\sqrt{s} = 1.935$ GeV. As the neutrons in that experiment were detected near the maximum laboratory angle, the momentum transfer of their events would be in the region where our value of $d\sigma/dt$ is high. The similarity with our results at this t makes it very unlikely that it is $\sqrt{s}$ that is the significant parameter.

If we view the variation of $d\sigma/dt$ with t as simply being due to a t-channel effect, then the fall at high t is not surprising except in its suddeness. In this context it is interesting to note that our results bear some resemblance to those of Harvey et al.[37] at 3.65 GeV/c for the reaction $\pi^- + p \rightarrow X^0 + n$, $X^0 \rightarrow 2\gamma$. Their results show some evidence of a maximum in $d\sigma/dt$ near $t = -0.4$ (GeV/$c)^2$, but the straightforward interpretation of their data is that $d\sigma/dt$ falls monotonically with increasing $-t$.

That the effects we see could be due to a final-state interaction, we consider to be very unlikely, not only because of the narrow X^0 width but also because $d\sigma/dt$ in that case should be only dependent on P^* or $\sqrt{s}$ which, as we have seen, is not in accord with the data.

The possibility of a systematic error in the technique of background subtraction must be considered. For example if a second resonance were present at a mass of about 980 MeV this could raise the assumed background level, so lowering the apparent X^0 cross section. To serve this pur-

pose such a resonance would need a width of less than 20 MeV whereas the preferred value of the $\pi_N(975)$ is about 60 MeV. It would also have to have a low cross section nearer threshold. In addition, much of the fall near bin 185 is already accounted for by the fall in the $\pi^+\pi^-$ channel at the K^+K^- threshold and there is no evidence for any other structure in the $\pi^+\pi^-$ channel between the K^+K^- threshold and the X^0.

In conclusion, while several effects may be present, the most likely interpretation is that the variation in $d\sigma/dt$ does represent a nonisotropic production angular distribution necessitating the presence of important partial waves up to $l = 2$. The total X^0 cross section rises from threshold at a rate $\sigma/P^* = 4K^*d\sigma/dt = 0.35 \pm 0.03$ μb/MeV/c. As already noted this is very small compared with the η or ω and this may help to explain how D waves could be relatively significant at a P^* of about 70 MeV/c.

The data above mass bin 187 (994.6 MeV) were interpreted in terms of ϕ meson production. The ϕ could be followed fairly easily above threshold, both for faster and slower neutrons, without the benefit of decay selection (Fig. 15). The design of a decay selection to take advantage of the large K^+K^- branching ratio was based on the near coplanarity of the two mesons with the beam axis together with their small opening angle. The problem in the selection was the possible disruption of the signature by a K meson which stopped in or

before a γ counter. If a K^- it would interact and if a K^+ it would decay. Either of these occur- rences could give rise to pulses in additional count- ers. Some allowance for such a possibility was made. The selection was used in the measure- ment of the width, to check the shape of the ϕ in the mass spectra, and as a check on the cross- section measurements. However, the efficiency of the selection is to some extent a function of the ϕ meson velocity and is difficult to determine in detail as several factors are involved. Therefore, there is an uncertain correction to cross-section measurements based on this selection.

Figure 19 shows the application of the threshold crossing technique at the ϕ. The time-of-flight gate chosen extended from 10.2 to 14.5 nsec. Note the greatly reduced background level resulting from the selection. From the ratio of the signals and the measured K^+K^- branching ratio the selec- tion efficiency for this channel at the ϕ mass was estimated to be $(51 \pm 5)\%$. The K^+K^- threshold occurs at bin 185 and the detection efficiency of the selection as a function of the effective mass of the K^+K^- pair is expected to rise sharply in the first two bins above this as the K^+K^- opening an- gle increases from zero. Much of the background persists below the K^+K^- threshold and is there- fore spurious. The residual K^+K^- background under the ϕ is clearly small.

The mass and width of the ϕ were extracted from this data over a range from bin 187 to 201. The

lower limit represented a compromise between the K^+K^- threshold and the need for several data points below the ϕ. Given the general near con- stancy of the background rate as a function of P_1, in the unselected events [Fig. 19(a)], a linear background had previously been used. This argu- ment for a linear background was not so justi- fied for the K^+K^- selection because of the threshold. However the measurement of the mass is rela- tively insensitive to assumption about the back- ground shape and the main interest in the deter- mination of the width was the comparison with the results from other, more accurate experiments. Also from observation most of the background under the ϕ in the selection was not in the K^+K^- channel and would be expected to be nearly con- stant with P_1. Therefore, a linear background was used and a quadratic background also tried as a check on the sensitivity to this assumption.

The best fit was obtained for the events in the K^+K^- selection at a mass value of 1019.4 ± 0.4 MeV ($\chi^2 = 11.5$ for 15 degrees of freedom). After al- lowing for the uncertainty in the momentum scale this became 1019.4 ± 0.7 MeV. A quadratic back- ground gave a similar result. For the width the corresponding results were 4.5 ± 1.1 and 3.9 ± 1.6 MeV. The mass value differs slightly from that earlier reported for the unselected events.[1] The more recent value is based on data with a much higher signal/background ratio and is therefore to be preferred.

Mass spectra for events with decay selection are shown in Fig. 20 for several t intervals and com- pared with Monte Carlo predictions. The general agreement between the two, apart from the rela- tive normalization, is good. The extraction of the cross section was straightforward. Figure 21 shows the t dependence obtained using both the selected and the unselected events. The selected events have the advantage of a much reduced background but there is some uncertainty in the selection efficiency. In the figure these points have been corrected using the efficiency previous- ly measured in the threshold crossing mode.

The general pattern is that of a predominantly S-wave cross section, with some evidence of a small decrease at high and low t. The compari- son with the ω again suggests that the effects of a final-state interaction with the decay products should be small. The KN cross sections are smaller in the relevant momentum range, the main final state consists of only two mesons and of course the lifetime is longer. S-wave produc- tion through the formation of an intermediate N^* state is not favored as the spin parity would have to be $\frac{1}{2}^-$ or $\frac{3}{2}^-$ and the nearest suitable baryon re- ported is again the $N^*(1700)$. At threshold the
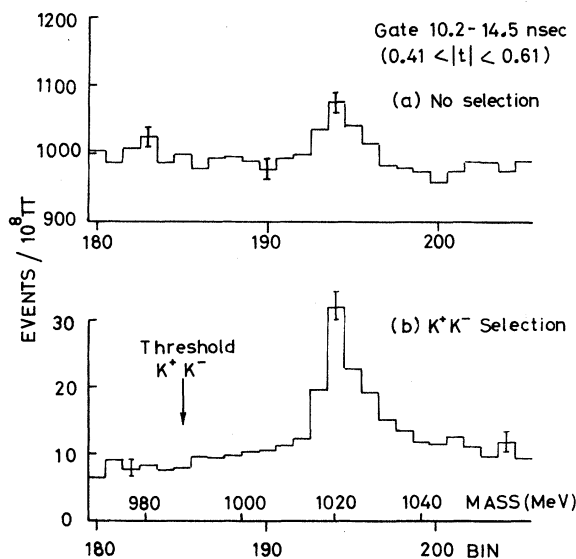

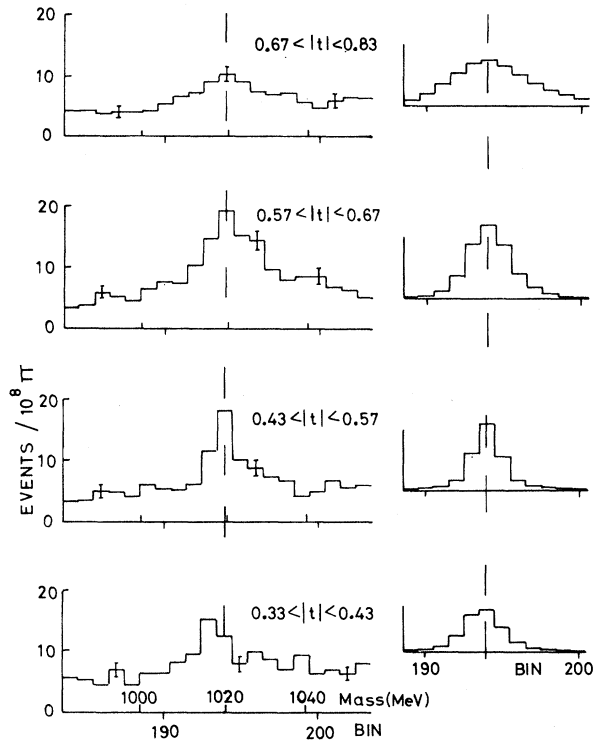FIG. 19. The yield of neutrons within the time-of- flight gate indicated as a function of beam momentum across the threshold for ϕ production. (a) shows the ϕ in missing mass, while in (b) a selection for the K^+K^- channel has been made.

FIG. 20. Mass spectra in the ϕ region, in four different t intervals, after making a selection for the K^+K^- channel. The corresponding S-wave predictions are shown on the right.

final-state energy required is about 1960 MeV. However, the width of this baryon is very uncertain and such a scheme is not impossible, especially in view of the low cross section involved.

Comparisons

In Table I we group together our results on the masses and widths of the four mesons and compare them also with the preferred values taken from the latest compilation of the Particle Data Group. As already noted, the accuracy of the mass scale, apart from statistical errors, is dominated by the accuracy in the absolute momentum measurements. The latter was estimated at 0.08% of P_1, but the only independent estimate of the accuracy comes from the mass scale. The comparison in Table I shows very good agreement at the X^0 and ϕ, reasonable agreement at the η and a possible disagreement, of 2.4σ, at the ω. An error in the absolute momentum of 0.1% P_1 would correspond to a shift in the mass at the ω of 0.6% MeV. But there is no systematic trend in the mass values obtained and no reason to make a general correction to the momentum scale. The ω is relatively wide compared with the other mesons. This makes the measured mass more sensitive to the effect of interference with the background. However, the observed distribution in the $\pi^+\pi^-\pi^0$ channel was well described by a Breit-Wigner distribution and showed no significant asymmetry (Fig. 12).

Generally good agreement is found for the measured widths. The apparent nonzero value for Γ_η is interpreted as a measure of the level at which the resolution of the apparatus is understood. The presence of an additional "tail" in the distribution of either P_1 or P_4 or θ_4 could explain the discrepancy (Fig. 10). But the magnitude of the effect is very small and only the exceptionally high cross section of the η coupled with the al-
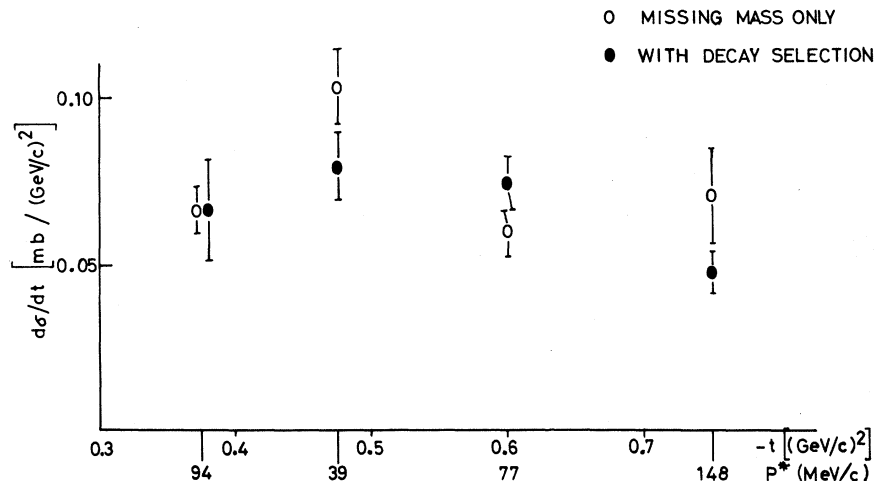

FIG. 21. Values for $d\sigma/dt$ for the ϕ. The open circles show the ϕ in missing mass only; the closed circles result from a K^+K^- selection after correcting for the selection efficiency. There is some indication of an increase in $d\sigma/dt$ close to threshold.

TABLE I. Masses and widths.

Meson	Mass (MeV) This expt.	Mass (MeV) P.D.G. [a]	Width (MeV) This expt.	Width (MeV) P.D.G. [a]
η	548.1 ± 0.4	548.8 ± 0.6	$(0.6^{\,b})$	0.002
ω	782.3 ± 0.6	783.9 ± 0.3	12.4 ± 2.2	10.0 ± 0.6
X^0	$957.1 \pm 0.6^{\,c}$	957.1 ± 0.6	< 1.9	$< 3.8^{\,d}$
ϕ	$1019.4 \pm 0.7^{\,c}$	1019.1 ± 0.5	4.5 ± 1.1	4.4 ± 0.3

[a] Particle Data Group, Phys. Lett. 39B, 1 (1972).
[b] Fit poor. See Fig. 10 and text.
[c] Final value of error, differs from Ref. 1 as estimated uncertainty in absolute value of P_1 has been increased from 0.05% to 0.08%.
[d] Reference 27.

TABLE II. Cross sections near threshold.

Meson	Form of $d\sigma/dt$	$d\sigma/dt$ [mb/(GeV/c)^2]	σ/P^* [μb/(MeV/c)]	$\frac{2}{3}\pi\lambda^2$ [a] (mb)
η	S + small P	12.3 ± 1.0	21.2 ± 1.8	4.3
ω	S + f.s.i. [b]	$3.5 \pm 0.3^{\,c}$	$8.3 \pm 0.7^{\,c}$	2.3
X^0	S, max at threshold	0.125 ± 0.010	0.35 ± 0.03	1.6
ϕ	S	0.097 ± 0.020	0.29 ± 0.06	1.5

[a] The S-wave unitarity limit in the $I = 0$ channel at threshold.
[b] Local minimum in $d\sigma/dt$ seen near threshold, attributed to a loss of ω's arising from a final-state interaction (f.s.i.) between decay π's and neutron.
[c] Corrected for effect described in footnote b. See Fig. 14 and text. Uncorrected values shown in Fig. 14(a).

most negligible background 2γ selection has enabled it to be detected. No correction to the measured values of Γ_ω and Γ_ϕ is necessary.

The results on the cross sections are summarized in Table II. Generally it appears that all four mesons have a relatively important S-wave component in the cross section near threshold, but the X^0 and ϕ cross sections are much smaller than those of η and ω. It is significant that the large cross section of the η is certainly associated with, and that of the ω is probably associated with an s-channel resonance close to threshold. A synthesis of these observations is provided by the picture advocated by Rosner[22] that meson-baryon systems can and do form resonances near threshold whenever a quark in one can annihilate an antiquark in the other. If the X^0 and ϕ are predominantly $\lambda\bar\lambda$ in quark structure this precludes them from forming such resonances with a nucleon and so accounts for their low cross sections compared to η and ω.

The presence of s-channel resonances in η and ω production seriously hinders any attempt to deduce the pseudoscalar and vector-meson mixing angles from our cross-section data. For instance the model of Alexander, Lipkin, and Scheck[38] is probably not valid when quark annihilation can occur and an analysis similar to that of Martin and Michael[39] based on t-channel dominance is also inappropriate in the presence of s-channel resonances.

VI. SUMMARY

We have described a form of missing-mass spectrometer designed to exploit the high mass resolution available close to threshold in a reaction of the form $1 + 2 \to 3 + 4$. Particle 4 is detected. This region is normally avoided in view of the rapidly varying density-of-states factor and other nonlinearities. It is shown that all such problems can be avoided by holding fixed the momentum

and angle of particle 4 and scanning in P_1. The only quantity requiring accurate measurement is then P_1 itself, although stability in the detection of particle 4 is also very important.

The method has been applied in the reaction $\pi^- + p \to x^0 + n$ using a momentum spectrometer to define the incident π^- and time of flight over 6.15 m to define the neutron. It has been used to investigate the η and ω and the meson spectrum around the $X^0(958)$ and the ϕ. It is found that such relatively narrow mesons can be studied in this manner and that the values for the masses and widths generally agree with and in some cases improve on the previous world average values. Evidence was found for a sharp drop in the $\pi^+\pi^-$ channel at a mass of 1.5 ± 1.5 MeV above the threshold for production of K^+K^- pairs. This is assumed to be associated with the effect previously reported by Alston-Garnjost *et al.*[35] and Grayer *et al.*[36]

Cross sections for the production of the resonances have been extracted. The results are most conveniently described in terms of $d\sigma/dt$. The integration over the resonance width, necessary to obtain the cross section, is made by integrating over the corresponding small range in P_1. These cross sections are being measured within a few MeV/c of threshold. Since a constant $d\sigma/dt$ is equivalent to an S-wave cross section with $\sigma \propto P^*$, the form of $d\sigma/dt$ as a function of t gives not only the initial S-wave component but also shows how this is modified as P^* increases. All four mesons are produced in an initial S wave; the η and X^0 show significant departures at higher P^* and the ω at very low P^*. The latter is attributed to a final-state interaction between the neutron and the ω decay products.

ACKNOWLEDGMENTS

would like to thank S.G.F. Frank, R. F. George, A. R. Faruqi, M. E. Kay, P. J. Nicholson, and J. G. Wilson for their help in the initial stages of this experiment. We are particularly indebted to

R. J. Gray at the Laboratory and R. F. Hobbs, D. G. Miller, and D. J. Scholes at Imperial College.

*Now at CERN, Geneva, Switzerland.

†Now at Banaras Hindu University, India.

[1]D. M. Binnie et al., Phys. Lett. 39B, 275 (1972).

[2]B. Maglić and G. Gosta, Phys. Lett. 18, 185 (1965).

[3]For example, see N. N. Focacci et al., Phys. Rev. Lett. 17, 890 (1966); D. Bowen et al., Phys. Rev. Lett. 26, 1663 (1971).

[4]For example, see H. Benz et al., Phys. Lett. 28B, 233 (1968).

[5]A. I. Baz, Zh. Eksp. Teor. Fiz. 40, 1511 (1961) [Sov. Phys.—JETP 13, 1058 (1961)].

[6]W. G. Jones et al., Phys. Lett. 23, 597 (1966).

[7]A. W. Hendry and R. G. Moorhouse, Phys. Lett. 18, 171 (1965).

[8]R. K. Adair, Rev. Mod. Phys. 37, 473 (1965).

[9]D. M. Binnie and A. Duane, Nucl. Instrum. Meth. 77, 329 (1970).

[10]D. G. Crabb et al., Nucl. Instrum. Meth. 48, 87 (1967).

[11]R. J. Kurz, UCRL Report No. 11339, 1964 (unpublished).

[12]For a detailed description of the decay system and its performance see M. E. Kay, Ph.D. thesis, Univ. of London, 1972 (unpublished). We acknowledge a very helpful comment from P. Sonderegger concerning γ identification.

[13]C. A. Baker et al., Nucl. Instrum. Meth. 59, 125 (1968).

[14]C. Bemporad et al., Phys. Lett. 25B, 380 (1967).

[15]S. Buniatov et al., presented to the International Conference on High Energy Physics, Heidelberg, 1967 (unpublished). The distribution is also shown in G. Salvini, Riv. Nuovo Cimento 1, 57 (1969).

[16]W. B. Richards et al., Phys. Rev. Lett. 16, 1221 (1966).

[17]M. A. Abolins et al., presented to the International Conference on High Energy Physics, Heidelberg, 1967 (unpublished).

[18]R. Kraemer et al., Phys. Rev. 136, B496 (1964).

[19]F. Uchiyama Campbell and R. K. Logan, Phys. Rev. 149, 1220 (1966).

[20]D. J. Herndon, A. Barbaro-Galtieri, and A. H. Rosenfeld, UCRL Report No. 20030 πN, 1970 (unpublished).

[21]S. Almehed and C. Lovelace, Nucl. Phys. B40, 157 (1972).

[22]J. Rosner, Phys. Rev. D 6, 2717 (1972).

[23]A. Brandstetter et al., Nucl. Phys. B39, 13 (1972).

[24]R. Aaron, R. D. Amado, and R. R. Silbar, Phys. Rev. Lett. 26, 407 (1971).

[25]J. P. Dufey et al., Phys. Lett. 26B, 410 (1968).

[26]P. M. Dauber et al., Phys. Rev. Lett. 13, 449 (1964).

[27]J. S. Danburg et al., in Experimental Meson Spectroscopy—1972, proceedings of the Third International Conference on Experimental Meson Spectroscopy, Philadelphia, 1972, edited by A. H. Rosenfeld and Kwan-Wu Lai (A.I.P., New York, 1972), p. 91.

[28]O. I. Dahl et al., Phys. Rev. 163, 1377 (1967).

[29]V. E. Balakin et al., Phys. Lett. 34B, 328 (1971).

[30]M. Aguilar-Benitez et al., Phys. Rev. Lett. 25, 1635 (1970); B. Maglić et al., ibid. 27, 1479 (1971).

[31]D. L. Cheshire et al., Phys. Rev. Lett. 28, 520 (1972).

[32]W. Kienzle et al., Phys. Lett. 19, 438 (1965).

[33]See review Particle Data Group, Phys. Lett. 39B, 1 (1972). H. W. Atherton et al., Phys. Lett. 43B, 249 (1973).

[34]S. M. Flatté et al., Phys. Lett. 38B, 232 (1972).

[35]M. Alston-Garnjost et al., Phys. Lett. 36B, 152 (1971).

[36]G. Grayer et al., in Experimental Meson Spectroscopy (Ref. 27), p. 5.

[37]E. H. Harvey et al., Phys. Rev. Lett. 27, 885 (1971).

[38]G. Alexander, H. J. Lipkin, and F. Scheck, Phys. Rev. Lett. 17, 412 (1966).

[39]A. D. Martin and C. Michael, Phys. Lett. 37B, 513 (1971).